Journal of Computational Physics 228 (2009) 6811–6832

Contents lists available at ScienceDirect

Journal of Computational Physics

journal homepage: www.elsevier.com/locate/jcp

A high-order low-dispersion symmetry-preserving finite-volume method for compressible flow on curvilinear grids

J.C. Kok

National Aerospace Laboratory NLR, Flight Physics and Loads Department, P.O. Box 90502, 1006 BM Amsterdam, The Netherlands

ARTICLE INFO

Article history:
Received 15 December 2008
Received in revised form 5 May 2009
Accepted 7 June 2009
Available online 23 June 2009

MSC:
65M06
76M12
76F65

Keywords:
Finite-volume
Curvilinear grids
Compressible flow
High-order discretization
Conservation properties
Skew-symmetric form
Low dispersion
Large-Eddy Simulation

ABSTRACT

A new high-order finite-volume method is presented that preserves the skew symmetry of convection for the compressible flow equations. The method is intended for Large-Eddy Simulations (LES) of compressible turbulent flows, in particular in the context of hybrid RANS–LES computations. The method is fourth-order accurate and has low numerical dissipation and dispersion. Due to the finite-volume approach, mass, momentum, and total energy are locally conserved. Furthermore, the skew-symmetry preservation implies that kinetic energy, sound-velocity, and internal energy are all locally conserved by convection as well. The method is unique in that all these properties hold on non-uniform, curvilinear, structured grids. Due to the conservation of kinetic energy, there is no spurious production or dissipation of kinetic energy stemming from the discretization of convection. This enhances the numerical stability and reduces the possible interference of numerical errors with the subgrid-scale model. By minimizing the numerical dispersion, the numerical errors are reduced by an order of magnitude compared to a standard fourth-order finite-volume method.

1. Introduction

The last decade has seen the advance of hybrid computational methods for turbulent flows that combine Large-Eddy Simulations (LES) in separated flow regions with the solution of the Reynolds-Averaged Navier–Stokes (RANS) equations for the attached boundary layers and other near-wall regions. This development was started by Spalart et al. [1] with the presentation of the Detached Eddy Simulation approach. Commonly, these hybrid RANS–LES methods are introduced in existing CFD solvers that are based on second-order finite-volume methods, in particular for compressible flows. It can be argued, however, that second-order accuracy is not sufficient for LES [2–4]. Numerical errors introduced by the discretization of the convection terms can be of the same order of magnitude as the subgrid-scale (SGS) stresses [3], in particular if a filter width equal to the mesh width is used. In that case, the computational results are determined as much by the numerical errors as by the SGS model. Although in some cases, these numerical errors and SGS modelling errors may partly cancel [5], thus improving the total accuracy of the computational result, this is not something that can be relied on in general. The possibly strong effect of the numerical errors on the results should somehow be taken into account. This paper aims

E-mail address: jkok@nlr.nl

0021-9991/$ - see front matter © 2009 Elsevier Inc. All rights reserved.
doi:10.1016/j.jcp.2009.06.015

at minimizing the interference of numerical errors with the SGS model. Thus, an opposite approach is followed compared to methods like MILES [6], in which one relies on the numerical dissipation to do the work of an SGS model.

A new high-order cell-centred finite-volume method for the compressible flow equations is presented that has the following key properties; it is the *combination* of these key properties that makes the method unique:

- Mass, momentum, and total energy are *locally* conserved.
- Kinetic energy, sound-velocity, and internal energy are *locally* conserved by convection.
- The inviscid terms are discretized with fourth-order accuracy in space.
- The method has low numerical dispersion.
- The method has no numerical dissipation (unless explicitly added).
- The first five properties are all maintained on smooth, *non-uniform, curvilinear* grids.

The grid is required to be smooth only for formal fourth-order accuracy (where a grid is considered smooth if it is the image of a uniform grid in computational space by a continuously differentiable mapping). The conservation properties, however, are independent of the grid smoothness.

These key properties are important for reducing the interference of numerical errors with the SGS model. In particular, local conservation of kinetic energy by convection implies that the discretized convection terms do not introduce spurious production or dissipation of kinetic energy, so that kinetic energy is only dissipated by the SGS (or viscous) stresses. Furthermore, minimizing numerical dispersion is equivalent to minimizing the implicit filter introduced by discretizing the convection terms, as will be shown below.

In this paper, the new high-order finite-volume method is derived in detail. Its basic ideas have been presented before [7]. Results are presented here for two basic test cases that will demonstrate the key properties of the method: the convection of an isentropic vortex and decaying isotropic homogeneous turbulence. The method already has been applied successfully to hybrid RANS–LES computations using the eXtra-Large Eddy Simulation (X-LES) method [8]. In particular, the improvement of the numerical accuracy over a standard second-order method has been shown for the turbulent flow over a rounded bump in a square duct [9].

1.1. Local conservation and high-order schemes

The Navier–Stokes equations are based on the conservation laws for mass, momentum, and total energy. Furthermore, the convection process by itself conserves both kinetic and internal energy (whereas pressure work and viscous dissipation cause an exchange of these energies). Numerical methods can preserve conservation in two ways: *globally*, if the total amount of a quantity in the flow domain is conserved, and *locally*, if it is based on a discrete divergence form with unique fluxes between adjacent grid cells. Local conservation is sufficient but not necessary for global conservation.

Numerical methods that preserve the *global* conservation of momentum and kinetic energy by convection for *incompressible* flow are common in the literature. Global conservation of kinetic energy ensures numerical stability because the total kinetic energy is an energy norm that cannot increase (but only decrease due to viscous dissipation). Thus, no numerical dissipation is needed to stabilize the method, which would otherwise reduce the numerical accuracy (and could interfere with the SGS model). As discussed by Kravchenko and Moin [3], such methods are based on the so-called skew-symmetric form of convection, which is defined as the average of the divergence and advective forms. Global conservation can then be derived if the discretization scheme satisfies a summation-by-parts rule (i.e., allows integration by parts in a discrete sense), which is the case for central differences and spectral methods, at least on uniform Cartesian grids [10]. Additionally, the skew-symmetric form reduces the aliasing errors compared to the divergence and advective forms [11,3]. Generally, however, these schemes *do not* conserve momentum (or kinetic energy) *locally*. This would require the discretized skew-symmetric form to be equivalent to a discrete divergence form. This depends on the discretization scheme satisfying a discrete product rule of differentiation, which is not the case for standard finite differences (and for spectral schemes only if de-aliased).

The staggered second-order finite-difference method of Harlow and Welch [12] *does* conserve both momentum and kinetic energy *locally* for incompressible flow (full conservation). It is based on a discrete divergence form of convection that can be shown to be equivalent to the skew-symmetric form by using a special product rule [13]. Morinishi et al. [13] have extended this method to fourth-order accuracy for both regular and staggered approaches on uniform grids. They also consider non-uniform grids, but state that one must choose between strict conservation or strict fourth-order accuracy. Vasilyev [14] has improved the method of Morinishi et al. for non-uniform grids, combining the fourth-order accuracy with the conservation of either momentum or kinetic energy, but not both. The staggered method of Verstappen and Veldman [15–17], on the other hand, maintains both fourth-order accuracy and full conservation on non-uniform Cartesian grids. The essential point is that they use Richardson extrapolation to derive the high-order scheme and that they *do not change the coefficients of the stencil* when applying the scheme to non-uniform grids. This means that the equations are discretized in computational space rather than physical space and that a smooth mapping between the two spaces is assumed (where the smooth mapping is only necessary for strict fourth-order accuracy and not for strict conservation). Attempts to minimize the local truncation errors in physical space on non-uniform grids by modifying the coefficients of the scheme will lead to loss of conservation of kinetic energy. It can even have a strongly adverse effect on the global discretization error [18,19]. Thus far, no one has presented an extension of these methods to curvilinear grids while maintaining both accuracy and conservation.

For *compressible* flow, a skew-symmetric form has been defined by Feiereisen et al. [20] that also leads to *global* conservation of momentum and kinetic energy by convection for standard central finite-difference and spectral methods, in the same manner as for incompressible flow. Formally, numerical stability is not ensured, however, since compression or expansion of the fluid results in an isentropic exchange of kinetic and internal energy (through work done by the pressure), allowing for an increase (as well as decrease) of total kinetic energy. Nevertheless, spurious production or dissipation of kinetic energy due to discretization of the convective terms is avoided. Based on the skew-symmetric form of Feiereisen et al. [20], Honein and Moin [21] have developed a sixth-order compact finite-difference scheme that locally conserves mass and globally conserves momentum and kinetic energy (by convection) as well as entropy and its square. Their method is stable without any artificial dissipation or filtering for the computation of decaying isotropic homogeneous turbulence at high Reynolds numbers. Momentum and total energy, however, are not locally conserved. Furthermore, non-uniform or curvilinear grids are not considered.

Local conservation of mass, momentum, and total energy is an essential property of numerical methods for compressible flows if one wants to capture weak solutions accurately. In other words, there must be a unique flux between two (adjacent) grid cells, sometimes also called the telescopic property. Ducros et al. [22] have developed high-order finite-difference and finite-volume methods that have this property and that are equivalent to a discrete skew-symmetric or skew-symmetric-like form, respectively (based on a discrete product rule). They do not try to conserve kinetic energy, however, but use the skew-symmetric(-like) forms because they reduce aliasing errors. Possibly, their finite-difference method locally conserves kinetic energy (although they do not show this and it is also not clear whether they use the form of Feiereisen), but their finite-volume method certainly does not. On non-uniform grids, they only consider the finite-volume method (as they could not obtain a conservative finite-difference method in that case). They extend the stencil of the fluxes only in one direction, however, so that the method is formally not fourth-order accurate in multiple dimensions. Furthermore, the truncation error in physical space is minimized by a mesh-size dependent interpolation that would also lead to the loss of kinetic-energy conservation (if it had been the case on a uniform grid in the first place). Others have used skew-symmetric forms for compressible flows also with the aim of reduced aliasing errors rather than conserving kinetic energy [23–26].

In deriving the present high-order finite-volume method, the following two essential points will be shown:

(1) Discrete local conservation of both momentum and kinetic energy by convection (full conservation) is possible for compressible flow, even on non-uniform curvilinear grids.
(2) Strict fourth-order accuracy can be obtained on non-uniform curvilinear grids without sacrificing full conservation.

For the first point, an alternative definition of the compressible skew-symmetric form of convection is given that is in-line with the incompressible definition. A discrete product rule is derived for finite-volume methods on curvilinear grids. Using this product rule, the discrete skew-symmetric form is shown to be equivalent to a discrete divergence form. This discrete form is used in the momentum equation and in the sound-velocity equation. Thus, mass, momentum, total energy, kinetic energy, sound-velocity, and internal energy are all locally conserved by convection. For the second point, the Richardson extrapolation approach of Verstappen and Veldman [17] is extended from staggered, Cartesian grids to cell-centred, curvilinear grids. Although this approach combines multiple control volumes, it will be shown that the method can be written in a form with unique fluxes between adjacent grid cells (telescopic property).

1.2. Numerical dissipation and dispersion

The aim of the high-order finite-volume method is to minimize the interference of numerical errors, stemming from the inviscid terms, with the SGS model. The SGS stresses are essentially responsible for dissipating the turbulent structures at small wave lengths close to the filter width. Reducing the interference of numerical errors with the SGS model therefore requires a numerical method with low numerical dispersion and dissipation at large wave numbers. Using a central stencil ensures that the scheme has no numerical dissipation for linear terms; for the non-linear convection term, numerical dissipation of kinetic energy is prevented by using the skew-symmetric form, as discussed above.

The numerical dispersion at large wave numbers can be minimized by using appropriate central finite-differencing schemes such as, in particular, the dispersion-relation preserving (DRP) scheme of Tam and Webb [27] and the compact schemes of Lele [28]. Tam and Webb create the freedom to minimize the dispersion by using a larger stencil than necessary to obtain fourth-order accuracy (seven instead of five points). Lele uses implicit differences to increase the order of accuracy and lower the dispersion without increasing the stencil of the scheme (but at the expense of solving an implicit system in each direction). Compact finite-difference schemes have been used frequently for LES [21,24,29]; this does not seem to be the case for the DRP scheme.

Compact finite-difference schemes have been extended to non-uniform, curvilinear grids [30,31]. To maintain (local) conservation of mass, momentum, and total energy on such grids, the finite-differencing must be applied to the equations written in strong conservation form in curvilinear coordinates. Visbal and Gaitonde [31,29] have done this successfully for a high-order compact scheme. Their scheme does not conserve kinetic energy, however, and it requires filtering to damp numerical instabilities introduced by grid non-uniformity, boundary conditions, and the non-linear terms. Similarly, compact schemes have been developed for finite-volume methods [32–36], again ensuring local conservation of mass, momentum, and total energy, but not of kinetic energy. These methods also typically require filtering to maintain numerical stability.

The DRP approach of Tam and Webb has been applied to finite-volume methods in the context of computational aeroacoustics. Nance et al. [37] did this by extending the stencil of the fluxes in one direction. This means that the fourth-order accuracy is lost on non-uniform grids in multiple dimensions. Furthermore, an upwind instead of a central stencil is used, introducing numerical dissipation. Popescu et al. [35] also apply the DRP approach to a finite-volume method such that the finite-volume method is equivalent to the DRP scheme on a uniform Cartesian grid. It has the same limitation as the method of Nance in multiple dimensions.

In the finite-volume method presented here, the DRP approach is applied to reduce the numerical dispersion. The freedom to minimize the dispersion is obtained by using a larger stencil in the Richardson extrapolation rather than using a larger stencil in the fluxes. On a uniform Cartesian grid, the method is essentially equivalent to the DRP scheme. For non-uniform, curvilinear grids, the following (third) essential point will be shown:

(3) Low dispersion (in the DRP sense) can be obtained on non-uniform curvilinear grids while maintaining full local conservation and high-order accuracy.

2. Symmetry and conservation for compressible flow

2.1. The skew-symmetric form of the convective operator

In Section 3, a high-order finite-volume method for the compressible flow equations will be presented that preserves not only the local conservation of mass, momentum, and total energy, but also the local conservation by convection of kinetic energy, sound-velocity, and internal energy. For this purpose, the skew-symmetric form of the convective operator is defined in this section. In particular, a definition is given for compressible flow that is in-line with the incompressible definition. This form is essential in deriving the high-order finite-volume method with the desired conservation properties.

Convection of a physical quantity, like mass, momentum, and energy, can be described by several forms of the convective operator. The divergence form of the operator, expressing conservation, is given by

$$D\phi \equiv \frac{\partial \rho\phi}{\partial t} + \nabla\cdot(\rho\boldsymbol{u}\phi) \quad (=0), \tag{1}$$

with $\phi(t,\boldsymbol{x})$ the convected physical quantity per unit mass, ρ the density and $\boldsymbol{u}$ the fluid velocity (and where $D\phi = 0$ holds if ϕ is only convected). The advective form,

$$A\phi \equiv \rho\frac{\partial \phi}{\partial t} + \rho\boldsymbol{u}\cdot\nabla\phi \quad (=0), \tag{2}$$

gives the time derivative of ϕ while moving along with a fluid particle (multiplied by density). The two forms are easily shown to be analytically equivalent using the continuity equation for a compressible flow,

$$\frac{\partial \rho}{\partial t} + \nabla\cdot(\rho\boldsymbol{u}) = 0, \tag{3}$$

which expresses mass conservation (and is obtained by setting $\phi = 1$ in $D\phi = 0$).

Convection of a physical quantity implies conservation not only of the quantity itself, but also of its quadratic form (ϕ^2), since

$$D\left(\frac{1}{2}\phi^2\right) = \frac{1}{2}\phi D\phi + \frac{1}{2}\phi A\phi = \phi K\phi \quad (=0), \tag{4}$$

where, in-line with the incompressible definition, the skew-symmetric form of the convective operator is defined as $K = \frac{1}{2}(D + A)$. Thus, conservation of the quadratic form ($D(\frac{1}{2}\phi^2) = 0$) follows immediately if the skew-symmetric form is used to express convection ($K\phi = 0$). If the divergence form ($D\phi = 0$) or the advective form ($A\phi = 0$) is used, then also the continuity equation is needed to derive the conservation of the quadratic form. The fact that K is a skew-symmetric operator follows from the more general relation

$$D(\phi\theta) = \phi D\theta + \theta A\phi = \phi K\theta + \theta K\phi, \tag{5}$$

which also shows that D and $-A$ are adjoint operators [38]. Besides the skew-symmetric form also a symmetric operator is defined naturally as $S = \frac{1}{2}(D - A)$, so that $D = K + S$ and $A = K - S$. Substituting the definitions of D and A, the skew-symmetric and symmetric operators are found to be

$$K\phi \equiv \frac{1}{2}\frac{\partial \rho\phi}{\partial t} + \frac{1}{2}\rho\frac{\partial \phi}{\partial t} + \frac{1}{2}\nabla\cdot(\rho\boldsymbol{u}\phi) + \frac{1}{2}\rho\boldsymbol{u}\cdot\nabla\phi, \tag{6a}$$

$$S\phi \equiv \frac{1}{2}\left(\frac{\partial \rho}{\partial t} + \nabla\cdot(\rho\boldsymbol{u})\right)\phi. \tag{6b}$$

Note that it follows from the continuity equation that the symmetric operator S is identical to zero, and that therefore the divergence form D, the advective form A, and the skew-symmetric form K of the convective operator are all equivalent.

The present definition of the skew-symmetric form, Eq. (6a), is suitable for deriving a finite-volume method with the desired *local* conservation properties. The skew-symmetric form introduced by Feiereisen et al. [20], given by

$$K_F\phi \equiv \frac{\partial \rho\phi}{\partial t} + \frac{1}{2}\nabla\cdot(\rho\boldsymbol{u}\phi) + \frac{1}{2}\rho\boldsymbol{u}\cdot\nabla\phi + \frac{1}{2}\phi\nabla\cdot(\rho\boldsymbol{u}), \tag{7}$$

has been used for deriving finite-difference and spectral methods with *global* kinetic-energy conservation [20,21]. The difference between the skew-symmetric form of Feiereisen K_F and the present definition K is the symmetric operator S, i.e., $K_F = K + S$.

Note that in both definitions of the skew-symmetric form, the density ρ goes together with the velocity $\boldsymbol{u}$ and not with ϕ. Sometimes the reverse is done [24,39]. It is essential, however, to keep the density with the velocity in order to obtain discrete kinetic-energy conservation, as will be seen below, and as was also pointed out by Honein and Moin [21]. This may seem counter-intuitive, as one could think that $\rho\phi$ is the conserved quantity that is convected by the velocity $\boldsymbol{u}$. Convection, however, conserves the physical quantities of a fluid particle. As a fluid particle has a constant mass, and not a constant volume, the quantities per unit mass are conserved (ϕ) and not the quantities per unit volume ($\rho\phi$).

2.2. The compressible flow equations

Now, the compressible flow equations can be written using the skew-symmetric form. Only the convective terms need to be considered. Therefore, we may limit ourselves to the compressible Euler equations. The equations for momentum and sound-velocity are given by

$$D\boldsymbol{u} + \nabla p = 0 \quad \text{or} \quad K\boldsymbol{u} + \nabla p = 0, \tag{8a}$$

$$Dc + \frac{\gamma-1}{2}\rho c\nabla\cdot\boldsymbol{u} = 0 \quad \text{or} \quad Kc + \frac{\gamma-1}{2}\rho c\nabla\cdot\boldsymbol{u} = 0, \tag{8b}$$

using either the divergence or skew-symmetric form, with p the pressure, c the sound-velocity, and γ the ratio of specific heats. Both analytic formulations will ultimately result in the same discrete formulation, as will be shown below. The kinetic energy is the quadratic form of the velocity vector, $E_k = \frac{1}{2}\boldsymbol{u}\cdot\boldsymbol{u}$, while the internal energy e can be interpreted as the quadratic form of the sound-velocity, since for a perfect gas $c^2 = \gamma p/\rho = \gamma(\gamma-1)e$. Equations for the kinetic and internal energy with convection in divergence form are obtained directly from the momentum and sound-velocity equations using the skew-symmetric form. Multiplying Eqs. (8a) and (8b) by $\boldsymbol{u}$ and c, respectively, and using Eq. (4), leads to

$$DE_k + \nabla\cdot(p\boldsymbol{u}) = p\nabla\cdot\boldsymbol{u}, \tag{9a}$$

$$De = -p\nabla\cdot\boldsymbol{u}. \tag{9b}$$

Thus, due to the skew symmetry of the convection operator in the momentum and sound-velocity equations, the left-hand sides of Eq. (9) obtain a divergence form, hence kinetic and internal energy are conserved by convection. The term on the right-hand sides of Eq. (9) represents the work done by the pressure as a consequence of compression or expansion of the fluid, leading to an (isentropic) exchange of kinetic and internal energy. Adding the equations for kinetic and internal energy shows that the total energy $E = e + E_k$ is conserved,

$$DE + \nabla\cdot(p\boldsymbol{u}) = 0. \tag{10}$$

For a numerical method that preserves the skew symmetry of convection in a discrete sense, the total energy will be globally conserved. In other words, the integral of total energy over the flow domain $\mathcal{D}$, given by

$$\int_{\mathcal{D}} \rho E \,\mathrm{d}V = \int_{\mathcal{D}} \rho\left(\frac{1}{2}\boldsymbol{u}\cdot\boldsymbol{u} + \frac{c^2}{\gamma(\gamma-1)}\right)\mathrm{d}V, \tag{11}$$

is conserved. For incompressible flows, the density is constant and therefore this integral is an energy norm of the velocity fields that cannot increase, proving the stability of such a symmetry-preserving method. For compressible flow, however, this integral is not strictly an energy norm and unbounded growth of the velocity fields is not excluded, because the density may approach zero. Nevertheless, the results below will show that such a symmetry-preserving method enhances the numerical stability for compressible flows. Additionally, in such a numerical method kinetic energy is locally conserved by convection, so that there is no spurious production or dissipation of kinetic energy stemming from the discretized convective operator, which could otherwise pollute the physical dissipation due to viscosity and the subgrid-scale model.

3. High-order finite-volume scheme

3.1. Conservative discretization preserving skew symmetry

A high-order finite-volume method for the compressible flow equations will be developed that preserves the local conservation by convection of momentum, kinetic energy, sound-velocity, and internal energy. The local conservation of

momentum, as well as mass and total energy, is simply ensured by applying a finite-volume discretization to the flow equations in divergence form. On the other hand, local conservation of kinetic and internal energy by convection is ensured if the skew symmetry of convection is preserved. This requires that the skew-symmetric form, rather than the divergence form, is used in the momentum and sound-velocity equations. Furthermore, the skew-symmetric form must be discretized such that Eq. (4) also holds in a discrete sense, where the left-hand side of this equation should be a finite-volume discretization of the divergence form. Finally, the two discretizations, one based on the divergence form and the other based on the skew-symmetric form, should be shown to be exactly equivalent, which involves the discretized continuity equation and a discrete product rule of differentiation, as will be shown below.

Starting point for deriving a high-order finite-volume scheme is a standard second-order scheme. Let the flow domain be discretized by a smooth, single-block, structured grid. A structured grid in 3D consists of an ordered set of hexahedral cells $\Omega_{\boldsymbol{i}}$, numbered by the triple index $\boldsymbol{i} = (i,j,k)$.

Essentially, a cell-centred, finite-volume discretization of the gradient operator $\nabla\mathcal{F}$ is obtained by integrating the gradient over the grid cell $\Omega_{\boldsymbol{i}}$ and applying Gauss' divergence theorem. This leads to

$$\nabla_{\boldsymbol{i}}\mathcal{F} = \frac{1}{V_{\boldsymbol{i}}}\sum_f \mathcal{F}_f \boldsymbol{A}_f, \tag{12}$$

with $V_{\boldsymbol{i}}$ the volume of the grid cell, $\mathcal{F}_f$ the flux at cell face f, and $\boldsymbol{A}_f$ the area vector of cell face f. The summation takes place over all faces f of the considered grid cell. Local conservation requires that the fluxes at the cell faces are unique. Uniform-flow consistency requires that the area vectors satisfy the geometric conservation law

$$\sum_f \boldsymbol{A}_f = 0. \tag{13}$$

The cell volume and the area vectors, satisfying the geometric conservation law, are computed from the cell-vertex coordinates by defining the edges of the grid cell as straight lines and by representing the cell by a trilinear interpolation function.

For a second-order central scheme, the fluxes are obtained by averaging the variables from the adjacent cells. When a flux consists of the product of several variables, one has to choose which variables are averaged. For this purpose, define the following averages

$$\bar{u}_f = \frac{1}{2}(u_{i,j,k} + u_{i+1,j,k}), \tag{14a}$$

$$\widetilde{uv}_f = \frac{1}{2}(u_{i,j,k}v_{i+1,j,k} + u_{i+1,j,k}v_{i,j,k}), \tag{14b}$$

where, without loss of generality, the face f between cells $\Omega_{i,j,k}$ and $\Omega_{i+1,j,k}$ is considered. Using the geometric conservation law (Eq. (13)), the following rules can be derived for the averages and for the discrete gradient operator (see Appendix A for details),

$$(\widetilde{uv})\widetilde{v}_f = \bar{u}_f\,\widetilde{v}\widetilde{v}_f, \tag{15a}$$

$$\nabla_{\boldsymbol{i}}\bar{u}\bar{v} = \frac{1}{2}\nabla_{\boldsymbol{i}}\overline{uv} + \frac{1}{2}\nabla_{\boldsymbol{i}}\widetilde{uv}, \tag{15b}$$

$$\nabla_{\boldsymbol{i}}\widetilde{uv} = u_{\boldsymbol{i}}\nabla_{\boldsymbol{i}}\bar{v} + v_{\boldsymbol{i}}\nabla_{\boldsymbol{i}}\bar{u}, \tag{15c}$$

where, for example, $\nabla_{\boldsymbol{i}}\bar{u}\bar{v}$ means that at each cell face f the flux is computed as $\mathcal{F}_f = \bar{u}_f\bar{v}_f$ and where the variables between brackets (uv) are averaged as one. The third rule is a discrete equivalent of the product rule of differentiation, which is essential in maintaining full conservation.

Eqs. (14) and (15) can be seen as an extension of the definitions and rules of Morinishi et al. [13] for finite-differencing methods on uniform grids to finite-volume methods on non-uniform grids. Considering non-uniform grids, Morinishi states that one needs to include the mesh size in the differencing and averaging operators such as Eq. (14) in order to maintain the numerical accuracy (in particular for high-order schemes). As a consequence, however, the discrete product rule no longer holds and full conservation cannot be maintained. Here, the discrete product rule does hold, because the grid metrics are not included in Eq. (14), but the averaging weights are kept constant (equal to $\frac{1}{2}$), following Verstappen and Veldman [17]. The metrics of non-uniform grids are only included through the cell volumes and area vectors in Eq. (12). How high-order accuracy can be obtained despite the grid-independent averaging weights will be shown in Section 3.3.

Local conservation is preserved if a finite-volume discretization of the divergence form D (Eq. (1)) is used, as given by

$$D_{\boldsymbol{i}}\phi \equiv \frac{\mathrm{d}\rho_{\boldsymbol{i}}\phi_{\boldsymbol{i}}}{\mathrm{d}t} + \nabla_{\boldsymbol{i}}\cdot\boldsymbol{F}, \tag{16}$$

with the discrete flux vector $\boldsymbol{F}$ equal to $\rho\boldsymbol{u}\phi$ obtained by some average of the variables from the adjacent cells. The discretization is locally conservative in the sense that there is a unique flux vector $\boldsymbol{F}$ at the face between two cells (telescopic property). The precise definition of the flux vector $\boldsymbol{F}$ is still open.

In order to preserve the skew symmetry (i.e., the local conservation by convection of the quadratic form ϕ^2), discretize the skew-symmetric form K (Eq. (6a)) as

$$K_{\boldsymbol{i}}\phi \equiv \frac{1}{2}\frac{\mathrm{d}\rho_{\boldsymbol{i}}\phi_{\boldsymbol{i}}}{\mathrm{d}t} + \frac{1}{2}\rho_{\boldsymbol{i}}\frac{\mathrm{d}\phi_{\boldsymbol{i}}}{\mathrm{d}t} + \frac{1}{2}\nabla_{\boldsymbol{i}}\cdot\overline{\rho\boldsymbol{u}\phi} + \frac{1}{2}\rho_{\boldsymbol{i}}\boldsymbol{u}_{\boldsymbol{i}}\cdot\nabla_{\boldsymbol{i}}\bar{\phi}. \tag{17}$$

Because the averaging weights in Eq. (14) have been chosen independent of the grid metrics and therefore the discrete product rule of differentiation (Eq. (15c)) holds, it follows that

$$\begin{aligned}\phi_{\boldsymbol{i}}K_{\boldsymbol{i}}\phi &= \frac{1}{2}\left(\phi_{\boldsymbol{i}}\frac{\mathrm{d}\rho_{\boldsymbol{i}}\phi_{\boldsymbol{i}}}{\mathrm{d}t} + \rho_{\boldsymbol{i}}\phi_{\boldsymbol{i}}\frac{\mathrm{d}\phi_{\boldsymbol{i}}}{\mathrm{d}t}\right) + \frac{1}{2}\left(\phi_{\boldsymbol{i}}\nabla_{\boldsymbol{i}}\cdot\overline{\rho\boldsymbol{u}\phi} + \rho_{\boldsymbol{i}}\boldsymbol{u}_{\boldsymbol{i}}\phi_{\boldsymbol{i}}\cdot\nabla_{\boldsymbol{i}}\bar{\phi}\right) = \frac{\mathrm{d}}{\mathrm{d}t}\left(\rho_{\boldsymbol{i}}\frac{1}{2}\phi_{\boldsymbol{i}}^2\right) + \frac{1}{2}\nabla_{\boldsymbol{i}}\cdot\phi(\widetilde{\rho\boldsymbol{u}}\phi)\\ &= \frac{\mathrm{d}}{\mathrm{d}t}\left(\rho_{\boldsymbol{i}}\frac{1}{2}\phi_{\boldsymbol{i}}^2\right) + \nabla_{\boldsymbol{i}}\cdot\left(\overline{\rho\boldsymbol{u}}\frac{1}{2}\widetilde{\phi\phi}\right).\end{aligned} \tag{18}$$

using also relation (15a) in the last step. Thus, Eq. (4) is preserved in a discrete sense, where the last line of Eq. (18) is a finite-volume discretization of the divergence form applied to ϕ^2, ensuring local conservation of ϕ^2.

Apparently, we now have two different discretizations of convection, one based on the divergence form (Eq. (16)), with local conservation of ϕ, and one based on the skew-symmetric form (Eq. (17)), with local conservation of ϕ^2. For a particular definition of the flux vector $\boldsymbol{F}$, however, the two forms are exactly equivalent, ensuring conservation of both ϕ and ϕ^2. Remember that the analytic divergence form D and skew-symmetric form K are related to each other by $D = K + S$ with S the symmetric form (Eq. (6b)). Require that the discrete divergence form $D_{\boldsymbol{i}}$ satisfies the relation $D_{\boldsymbol{i}} = K_{\boldsymbol{i}} + S_{\boldsymbol{i}}$ with the symmetric operator S, i.e., the continuity equation, discretized as

$$S_{\boldsymbol{i}}\phi \equiv \frac{1}{2}\left(\frac{\mathrm{d}\rho_{\boldsymbol{i}}}{\mathrm{d}t} + \nabla_{\boldsymbol{i}}\cdot\overline{\rho\boldsymbol{u}}\right)\phi_{\boldsymbol{i}}. \tag{19}$$

Using the rules of Eq. (15), one then finds that

$$D_{\boldsymbol{i}}\phi \equiv \frac{\mathrm{d}\rho_{\boldsymbol{i}}\phi_{\boldsymbol{i}}}{\mathrm{d}t} + \nabla_{\boldsymbol{i}}\cdot\overline{\rho\boldsymbol{u}}\bar{\phi}, \tag{20}$$

which is indeed a finite-volume discretization of the divergence form in the form of Eq. (16). Thus, if the discrete continuity equation is satisfied ($S_{\boldsymbol{i}} \equiv 0$), then the discrete divergence and skew-symmetric forms are equivalent. Eq. (20) shows that the flux vector $\boldsymbol{F}$ should be computed as $\overline{\rho\boldsymbol{u}}\bar{\phi}$. In other words, when computing the averages at the cell faces, ρ goes together with $\boldsymbol{u}$ and not with ϕ. This is essential in order to preserve the skew symmetry, as was also remarked at the end of Section 2.1. Note that this scheme differs only slightly from one of the variants of the Jameson scheme [40] in which the flux is computed by averaging the flow variables per unit volume $\boldsymbol{F} = \overline{\rho\boldsymbol{u}}\,\overline{\rho\phi}/\bar{\rho}$. In fact, for incompressible flow, this Jameson-type averaging is equivalent to the skew-symmetric form.

3.2. The compressible flow equations

A second-order finite-volume discretization of the compressible Euler equations, in which momentum, kinetic energy, sound-velocity, and internal energy are all locally conserved by convection, can now be derived by applying the discrete skew-symmetric, symmetric, and divergence forms as defined above (Eqs. (17), (19), and (20)). The continuity equation is discretized as in Eq. (19),

$$\frac{\mathrm{d}\rho_{\boldsymbol{i}}}{\mathrm{d}t} + \nabla_{\boldsymbol{i}}\cdot\overline{\rho\boldsymbol{u}} = 0. \tag{21}$$

This implies that $S_{\boldsymbol{i}} \equiv 0$, so that the discrete divergence and skew-symmetric forms are equivalent ($D_{\boldsymbol{i}} \equiv K_{\boldsymbol{i}}$). The momentum and sound-velocity equations are discretized using either of these forms as

$$D_{\boldsymbol{i}}\boldsymbol{u} + \nabla_{\boldsymbol{i}}\bar{p} \equiv K_{\boldsymbol{i}}\boldsymbol{u} + \nabla_{\boldsymbol{i}}\bar{p} = 0, \tag{22a}$$

$$D_{\boldsymbol{i}}c + \frac{\gamma-1}{2}\rho_{\boldsymbol{i}}c_{\boldsymbol{i}}\nabla_{\boldsymbol{i}}\cdot\bar{\boldsymbol{u}} \equiv K_{\boldsymbol{i}}c + \frac{\gamma-1}{2}\rho_{\boldsymbol{i}}c_{\boldsymbol{i}}\nabla_{\boldsymbol{i}}\cdot\bar{\boldsymbol{u}} = 0. \tag{22b}$$

Multiplying these equations with the velocity $\boldsymbol{u}_{\boldsymbol{i}}$ and the sound-velocity $c_{\boldsymbol{i}}$, respectively, and using Eq. (18) gives the discretized equations for the kinetic and internal energy,

$$\frac{\mathrm{d}\rho_{\boldsymbol{i}}(E_k)_{\boldsymbol{i}}}{\mathrm{d}t} + \nabla_{\boldsymbol{i}}\cdot(\overline{\rho\boldsymbol{u}}\tilde{E}_k) + \nabla_{\boldsymbol{i}}\cdot\widetilde{\boldsymbol{u}p} = p_{\boldsymbol{i}}\nabla_{\boldsymbol{i}}\cdot\bar{\boldsymbol{u}}, \tag{23a}$$

$$\frac{\mathrm{d}\rho_{\boldsymbol{i}}e_{\boldsymbol{i}}}{\mathrm{d}t} + \nabla_{\boldsymbol{i}}\cdot(\overline{\rho\boldsymbol{u}}\tilde{e}) = -p_{\boldsymbol{i}}\nabla_{\boldsymbol{i}}\cdot\bar{\boldsymbol{u}}, \tag{23b}$$

with $\tilde{E}_k = \frac{1}{2}\widetilde{\boldsymbol{u}\cdot\boldsymbol{u}}$ and $\gamma(\gamma-1)\tilde{e} = \widetilde{cc}$, and with the left-hand sides in conservative form. Finally, adding the discrete equations for kinetic and internal energy gives the equation for the total energy E in conservative form,

$$\frac{\mathrm{d}\rho_{\boldsymbol{i}} E_{\boldsymbol{i}}}{\mathrm{d}t} + \nabla_{\boldsymbol{i}} \cdot (\overline{\rho \boldsymbol{u}}\widetilde{E}) + \nabla_{\boldsymbol{i}} \cdot \widetilde{\boldsymbol{u}p} = 0, \tag{24}$$

with $\widetilde{E} = \widetilde{E_k} + \tilde{e}$.

When solving the semi-discrete equations, one has to choose which equations are integrated in time. For the momentum equation, one can choose either the divergence or the skew-symmetric form. For the energy equation, one can choose between the sound-velocity equation (in divergence or skew-symmetric form), the internal-energy equation, or the total-energy equation. If the time-integration is exact, all these different forms are exactly equivalent. Consistent with standard finite-volume methods for compressible flow, here the divergence forms of the momentum and total-energy equations are solved.

An alternative choice for the energy equation is presented by Honein and Moin [21]. They discretize the entropy equation using the skew-symmetric form, resulting in the conservation of entropy and its square, but at the loss of the conservation of internal and total energy. Although the present scheme does not conserve the entropy exactly, the results below will show that the entropy errors are small.

So far, only the spatial discretization has been considered. For the time-integration, one could also require that the skew symmetry is preserved, i.e., that Eq. (18) also holds with a discretized time derivative. This issue is considered in Appendix B. No suitable time-integration method has yet been found, however, that exactly maintains skew symmetry and conservation of kinetic energy for the compressible convection operator. Therefore, standard, accurate time-integration schemes are used. For the results presented below, either the explicit four-stage Runge–Kutta scheme or the implicit second-order backward scheme have been employed.

3.3. Basic fourth-order finite-volume scheme

A fourth-order finite-volume scheme on non-uniform curvilinear grids is derived by applying Richardson extrapolation [17] to the second-order discretization, while preserving the skew symmetry as in the previous sections. Consider again the second-order, cell-centred scheme for the gradient operator in $\mathbb{R}^d$ (with the spatial dimension $d = 1, 2$, or 3), written as

$$V_{\boldsymbol{i}}^h \nabla_{\boldsymbol{i}}^h \mathcal{F} = B_{\boldsymbol{i}}^h, \tag{25}$$

with the flux balance $B_{\boldsymbol{i}}^h$ given by

$$B_{\boldsymbol{i}}^h = F_{i+1/2,j,k}^h - F_{i-1/2,j,k}^h + F_{i,j+1/2,k}^h - F_{i,j-1/2,k}^h + F_{i,j,k+1/2}^h - F_{i,j,k-1/2}^h, \tag{26}$$

and with $F^h = \mathcal{F}^h \boldsymbol{A}^h$ the flux through a cell face. The superscript h indicates the mesh size in the computational domain.

The idea of Richardson extrapolation is to increase the order of accuracy by cancelling the leading-order errors of the discretization. To determine the leading-order errors, the equations are considered in the computational domain. A smooth, non-uniform grid can be interpreted as the image of a uniform grid with mesh size h in the computational domain $\xi \in [0,1]^d$ by the continuously differentiable mapping $\boldsymbol{x}(\xi)$ (where, without loss of generality, h is assumed to be the same in all computational directions). A finite-volume discretization can be interpreted as a discretization of the conservative form of the gradient operator in the curvilinear coordinate system ξ,

$$J\nabla\mathcal{F} = \sum_{j=1}^{d} \frac{\partial}{\partial \xi_j} (\mathcal{F} J \nabla \xi_j), \tag{27}$$

with $J = \det(\mathrm{d}\boldsymbol{x}/\mathrm{d}\xi)$ the determinant of the Jacobian of the transformation $\boldsymbol{x}(\xi)$. In particular, the cell volume $V_{\boldsymbol{i}}^h/h^d$ can be interpreted as a discretization of the Jacobian J and the area vectors $\boldsymbol{A}^h/h^{d-1}$ as discretizations of the metric terms $J\nabla\xi_i$ (see Fig. 1), and finally the flux balance $B_{\boldsymbol{i}}^h/h^d$ as a discretization of the right-hand side of Eq. (27) (which is also a flux balance). Because symmetric stencils are employed, the discretization errors contain only terms of even order in h. Hence, Eq. (25) divided by h^d can be interpreted as a second-order approximation to Eq. (27). This can be written as

$$\frac{1}{h^d} V_{\boldsymbol{i}}^h = J_{\boldsymbol{i}} + C_{\boldsymbol{i}} h^2 + \mathcal{O}(h^4), \tag{28a}$$

$$\frac{1}{h^d} B_{\boldsymbol{i}}^h = \left(\sum_{j=1}^{d} \frac{\partial}{\partial \xi_j} (\mathcal{F} J \nabla \xi_j) \right)_{\boldsymbol{i}} + D_{\boldsymbol{i}} h^2 + \mathcal{O}(h^4), \tag{28b}$$

with the coefficients C and D both functions of ξ. These formulas depend on Taylor series up to fifth order of the functions $\mathcal{F}(\xi)$ and $\boldsymbol{x}(\xi)$ for which it is sufficient that these functions are five times continuously differentiable. Note that on non-uniform grids, Vasilyev [14] also discretizes the gradient in computational space, but does not base it on the conservative form of Eq. (27) and as a consequence is not able to maintain full conservation.

To obtain a fourth-order scheme, the leading-order discretization errors of the second-order scheme should be annihilated. Following Verstappen and Veldman [17], this can be done by applying, at each cell centre, the same discretization stencil on a second, larger control volume and subsequently combining the two discretization stencils through Richardson extrapolation. Verstappen and Veldman used a staggered scheme, for which a control volume with a three times larger mesh

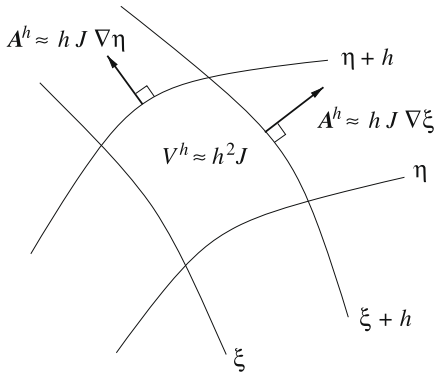

Fig. 1. Metric terms of a grid cell in a curvilinear coordinate system in 2D.

size in the computational domain was the smallest control volume allowing the same discretization stencil. For a cell-centred scheme, a control volume with twice the mesh size could be used, but its vertices would not coincide with grid points, so that its metrics could not be directly computed from the grid coordinates. Therefore, for the current cell-centred scheme, also a control volume with a three times larger mesh size in the computational domain is preferred initially.

Define for each cell centre a control volume $\Omega_{\boldsymbol{i}}^{3h}$ by joining the 3^d surrounding grid cells, as illustrated in Fig. 2. This control volume has a mesh size $3h$ in the computational domain. The volume V^{3h} and the area vectors $\boldsymbol{A}^{3h}$ of this control volume are defined in exactly the same manner as for the grid cell itself in terms of the vertices of the control volume $\Omega_{\boldsymbol{i}}^{3h}$. The same discretization stencil is applied to this control volume, which means that the stencil must now have a spacing of three mesh sizes (see again Fig. 2). This leads to

$$V_{\boldsymbol{i}}^{3h}\nabla_{\boldsymbol{i}}^{3h}\mathcal{F} = B_{\boldsymbol{i}}^{3h}, \tag{29}$$

with the flux balance given by

$$B_{\boldsymbol{i}}^{3h} = F_{i+3/2,j,k}^{3h} - F_{i-3/2,j,k}^{3h} + F_{i,j+3/2,k}^{3h} - F_{i,j-3/2,k}^{3h} + F_{i,j,k+3/2}^{3h} - F_{i,j,k-3/2}^{3h}. \tag{30}$$

The flux $F^{3h} = \mathcal{F}^{3h}\boldsymbol{A}^{3h}$ at the face f between control volumes $\Omega_{i,j,k}^{3h}$ and $\Omega_{i+3,j,k}^{3h}$ is computed in exactly the same manner as the fluxes of the original control volume, averaging the variables located at the centres of the two control volumes. Thus, the following averages are used:

$$\bar{u}_f^{3h} = \frac{1}{2}\left(u_{i,j,k} + u_{i+3,j,k}\right), \tag{31a}$$

$$\widetilde{uv}_f^{3h} = \frac{1}{2}\left(u_{i,j,k}v_{i+3,j,k} + u_{i+3,j,k}v_{i,j,k}\right). \tag{31b}$$

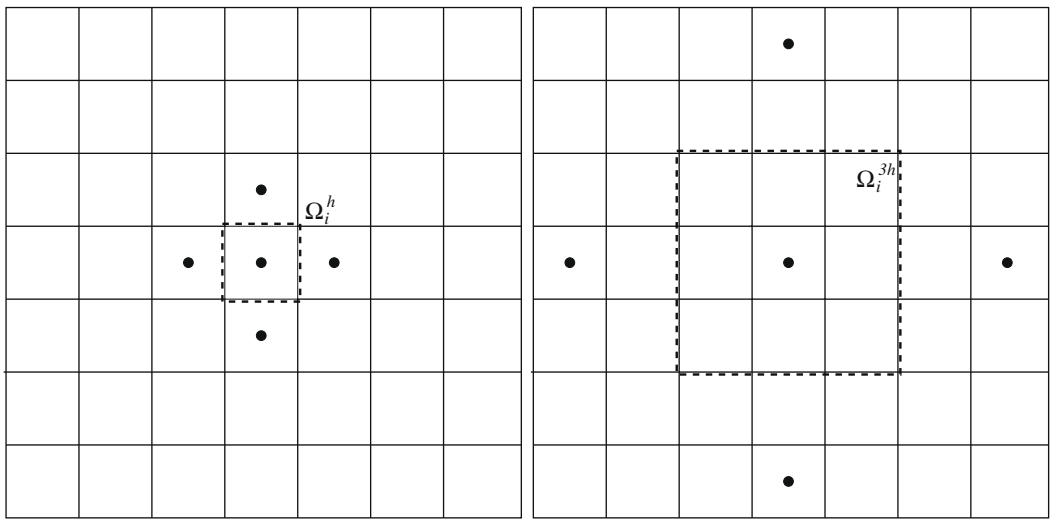

Fig. 2. Control volumes $\Omega_{\boldsymbol{i}}^{h}$ and $\Omega_{\boldsymbol{i}}^{3h}$ around the same cell centre with corresponding discretization stencils (2D).

Again the averaging weights (equal to $\frac{1}{2}$) are independent of the grid metrics, so that, for this second discrete gradient operator, the rules of Eq. (15) also apply.

The discretization stencil that is employed to define the cell volume and flux balance on the new control volume is exactly the same as on the original control volume, but using a three times larger mesh size. Therefore, the discretization errors for the new control volume are also given by Eq. (28), with the same values of the coefficients C and D for the leading-order discretization errors, but with the mesh size h replaced with $3h$. Thus, the leading-order errors are a factor 3^2 larger for the new control volume. Cancelling these leading-order errors through Richardson extrapolation results in a fourth-order accurate finite-volume discretization of the gradient operator, given by

$$V_{\boldsymbol{i}}^{*}\nabla_{\boldsymbol{i}}^{*}\mathcal{F} = B_{\boldsymbol{i}}^{*}, \tag{32}$$

with

$$V_{\boldsymbol{i}}^{*} = \frac{h^d}{3^2-1}\left(3^2\frac{1}{h^d}V_{\boldsymbol{i}}^{h} - \frac{1}{(3h)^d}V_{\boldsymbol{i}}^{3h}\right) = \frac{9}{8}V_{\boldsymbol{i}}^{h} - \frac{1}{8\cdot 3^d}V_{\boldsymbol{i}}^{3h}, \tag{33a}$$

$$B_{\boldsymbol{i}}^{*} = \frac{h^d}{3^2-1}\left(3^2\frac{1}{h^d}B_{\boldsymbol{i}}^{h} - \frac{1}{(3h)^d}B_{\boldsymbol{i}}^{3h}\right) = \frac{9}{8}B_{\boldsymbol{i}}^{h} - \frac{1}{8\cdot 3^d}B_{\boldsymbol{i}}^{3h}, \tag{33b}$$

where superscript * indicates the fourth-order discretization. The fourth-order discrete gradient operator can be written as a linear combination of the two second-order operators,

$$\nabla_{\boldsymbol{i}}^{*}\mathcal{F} = a_{\boldsymbol{i}}\nabla_{\boldsymbol{i}}^{h}\mathcal{F} + b_{\boldsymbol{i}}\nabla_{\boldsymbol{i}}^{3h}\mathcal{F}, \tag{34}$$

with the coefficients $a_{\boldsymbol{i}} = \frac{9}{8}V_{\boldsymbol{i}}^{h}/V_{\boldsymbol{i}}^{*}$ and $b_{\boldsymbol{i}} = -\frac{1}{8}V_{\boldsymbol{i}}^{3h}/(3^d V_{\boldsymbol{i}}^{*})$. For each grid cell, this scheme has a seven-point stencil in each computational direction (from $i-3$ to $i+3$, although cells $i-2$ and $i+2$ are not used).

To show that the scheme is locally conservative, the flux balance can be written as

$$B_{\boldsymbol{i}}^{*} = F_{i+1/2,j,k}^{*} - F_{i-1/2,j,k}^{*} + F_{i,j+1/2,k}^{*} - F_{i,j-1/2,k}^{*} + F_{i,j,k+1/2}^{*} - F_{i,j,k-1/2}^{*}, \tag{35}$$

with the fluxes defined uniquely at each cell face by

$$F_{i+1/2,j,k}^{*} = \frac{9}{8}F_{i+1/2,j,k}^{h} - \frac{1}{8\cdot 3^d}\left(F_{i-1/2,j,k}^{3h} + F_{i+1/2,j,k}^{3h} + F_{i+3/2,j,k}^{3h}\right). \tag{36}$$

A fourth-order discretization of the convective operator is obtained by using the fourth-order discrete gradient operator $\nabla_{\boldsymbol{i}}^{*}$, as defined above, in the definitions of the discrete skew-symmetric, symmetric, and divergence forms as given by Eqs. (17), (19), and (20). A fourth-order finite-volume scheme for the compressible Euler equations is obtained by applying these fourth-order operators in Eqs. (21)-(24).

The question now remains whether, for this fourth-order scheme, the conservation of both momentum and kinetic energy (as well as both sound-velocity and internal energy) can be proven. In other words, using the fourth-order gradient operator in the skew-symmetric and divergence forms (Eqs. (17) and (20)), can it still be proven that these two forms are equivalent and that Eq. (18) holds. The proofs given for the second-order scheme depend solely on the rules of Eq. (15). Thus, if these rules hold for the fourth-order scheme, then the conservation of both momentum and kinetic energy follows. Because the fourth-order discrete gradient operator is a linear combination of the two second-order operators and because the rules of Eq. (15) are linear in terms of the gradient, it follows that they also hold for the fourth-order gradient. For example, the discrete product rule of differentiation holds for both second-order gradients, i.e.,

$$\nabla_{\boldsymbol{i}}^{h}\widetilde{u\bar{v}} = u_{\boldsymbol{i}}\nabla_{\boldsymbol{i}}^{h}\bar{v} + v_{\boldsymbol{i}}\nabla_{\boldsymbol{i}}^{h}\bar{u}, \tag{37a}$$

$$\nabla_{\boldsymbol{i}}^{3h}\widetilde{u\bar{v}} = u_{\boldsymbol{i}}\nabla_{\boldsymbol{i}}^{3h}\bar{v} + v_{\boldsymbol{i}}\nabla_{\boldsymbol{i}}^{3h}\bar{u}, \tag{37b}$$

so that indeed

$$\nabla_{\boldsymbol{i}}^{*}\widetilde{u\bar{v}} \overset{(34)}{=} a_{\boldsymbol{i}}\nabla_{\boldsymbol{i}}^{h}\widetilde{u\bar{v}} + b_{\boldsymbol{i}}\nabla_{\boldsymbol{i}}^{3h}\widetilde{u\bar{v}} \overset{(37)}{=} u_{\boldsymbol{i}}(a_{\boldsymbol{i}}\nabla_{\boldsymbol{i}}^{h}\bar{v} + b_{\boldsymbol{i}}\nabla_{\boldsymbol{i}}^{3h}\bar{v}) + v_{\boldsymbol{i}}(a_{\boldsymbol{i}}\nabla_{\boldsymbol{i}}^{h}\bar{u} + b_{\boldsymbol{i}}\nabla_{\boldsymbol{i}}^{3h}\bar{u}) \overset{(34)}{=} u_{\boldsymbol{i}}\nabla_{\boldsymbol{i}}^{*}\bar{v} + v_{\boldsymbol{i}}\nabla_{\boldsymbol{i}}^{*}\bar{u}. \tag{38}$$

4. Numerical dispersion and dissipation

4.1. Low-dispersion high-order finite-volume scheme

As stated in the introduction, reducing the interference of numerical errors with the SGS model requires a numerical method with low numerical dispersion and dissipation at large wave numbers. Dissipation is minimized by using a central stencil and the skew-symmetric form for convection. To minimize dispersion, the ideas of Tam and Webb [27] are followed. Their dispersion-relation preserving (DRP) scheme uses finite-differencing to discretize the gradient operator. A symmetric,

seven-point stencil is used. The coefficients of the stencil have three degrees of freedom of which two are used to make the scheme fourth-order accurate and the remaining one is used to minimize the dispersion.

Thus, in order to minimize the numerical dispersion of the fourth-order finite-volume scheme as presented in the previous section, an additional degree of freedom is needed. The size of the discretization stencil should be increased while preserving the skew symmetry of the method. As seen in the previous section, the skew symmetry is preserved if a high-order scheme is defined as a linear combination of second-order discretizations using Richardson extrapolation. Therefore, an additional degree of freedom is created by introducing, at each cell centre, a third control volume. For this purpose, the control volume $\Omega_{\boldsymbol{i}}^{2h}$ with a mesh size of $2h$ in the computational domain (see Fig. 3) is used. Note that this control volume was initially not used in the basic fourth-order scheme, because it has its vertices located not at grid points, but at the centres of the grid cells. The smallest additional control volume with its vertices at grid points, however, has a mesh size of $5h$ in the computational domain. Using this control volume (instead of $\Omega_{\boldsymbol{i}}^{2h}$) would increase the width of the stencil from seven to eleven points in each direction. Using $\Omega_{\boldsymbol{i}}^{2h}$ keeps the width of the stencil equal to seven.

The discretization of the gradient operator on the control volume $\Omega_{\boldsymbol{i}}^{2h}$ can be written as

$$V_{\boldsymbol{i}}^{2h}\nabla_{\boldsymbol{i}}^{2h}\mathcal{F} = B_{\boldsymbol{i}}^{2h}, \tag{39}$$

with $V_{\boldsymbol{i}}^{2h}$ the volume of the control volume $\Omega_{\boldsymbol{i}}^{2h}$ and with the flux balance $B_{\boldsymbol{i}}^{2h}$ given by

$$B_{\boldsymbol{i}}^{2h} = F_{i+1,j,k}^{2h} - F_{i-1,j,k}^{2h} + F_{i,j+1,k}^{2h} - F_{i,j-1,k}^{2h} + F_{i,j,k+1}^{2h} - F_{i,j,k-1}^{2h}. \tag{40}$$

Again, the flux $F^{2h} = \mathcal{F}^{2h}\boldsymbol{A}^{2h}$ at the face f between control volumes $\Omega_{i,j,k}^{2h}$ and $\Omega_{i+2,j,k}^{2h}$ is computed in the exact same manner as the fluxes of the original control volume, averaging the variables located at the centres of the two control volumes. Combining all three discretization stencils through Richardson extrapolation to cancel the leading-order error in the computational domain, the following fourth-order finite-volume discretization of the gradient operator is found:

$$V_{\boldsymbol{i}}^{\beta}\nabla_{\boldsymbol{i}}^{\beta}\mathcal{F} = B_{\boldsymbol{i}}^{\beta}, \tag{41}$$

with

$$V_{\boldsymbol{i}}^{\beta} = \beta\left(\frac{4}{3}V_{\boldsymbol{i}}^{h} - \frac{1}{3\cdot 2^{d}}V_{\boldsymbol{i}}^{2h}\right) + (1-\beta)\left(\frac{9}{8}V_{\boldsymbol{i}}^{h} - \frac{1}{8\cdot 3^{d}}V_{\boldsymbol{i}}^{3h}\right), \tag{42a}$$

$$B_{\boldsymbol{i}}^{\beta} = \beta\left(\frac{4}{3}B_{\boldsymbol{i}}^{h} - \frac{1}{3\cdot 2^{d}}B_{\boldsymbol{i}}^{2h}\right) + (1-\beta)\left(\frac{9}{8}B_{\boldsymbol{i}}^{h} - \frac{1}{8\cdot 3^{d}}B_{\boldsymbol{i}}^{3h}\right), \tag{42b}$$

where the basic fourth-order discretization is recovered for $\beta = 0$. The parameter β can now be tuned to minimize the dispersion of the scheme. Considering a set of linear equations, a suitable value of β is obtained by requiring that the scheme reduces to the DRP scheme of Tam and Webb on a uniform Cartesian grid. For linear equations, averaging flow states to compute fluxes at cell faces is equivalent to averaging the fluxes themselves. On a uniform Cartesian grid, the flux balance then reduces to the following stencil for each computational direction separately:

$$B_{i}^{\beta} = a_1(F_{i+1} - F_{i-1}) + a_2(F_{i+2} - F_{i-2}) + a_3(F_{i+3} - F_{i-3}), \tag{43}$$

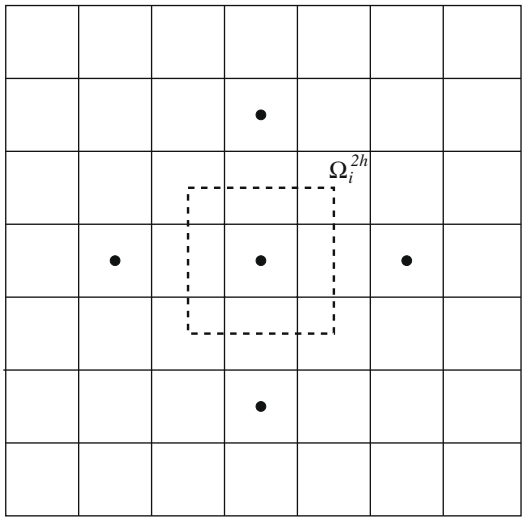

Fig. 3. Control volume $\Omega_{\boldsymbol{i}}^{2h}$ around the same cell centre as in Fig. 2 with corresponding discretization stencil (2D).

with the coefficients given by

$$a_1 = \frac{27+5\beta}{48}, \quad a_2 = -\frac{\beta}{12}, \quad a_3 = \frac{\beta-1}{48}. \tag{44}$$

In the DRP scheme, the same stencil is used for the flux balance, with the coefficients (as optimized by Tam [41]) given by

$$a_1 = 0.770882380518, \quad a_2 = -0.166705904415, \quad a_3 = 0.0208431427703. \tag{45}$$

Both sets of coefficients define a fourth-order scheme and the two sets are identical for

$$\beta = -12a_2 = 2.00047085298. \tag{46}$$

Thus, this value of β is used in Eq. (42b) for the flux balance. The results presented in Section 5.1 will show that this value of β is also suitable for the non-linear Euler equations using the skew-symmetric discretization (rather than flux averaging). In practice, the high-order cell volume has been computed as in the basic high-order finite-volume scheme (Eq. (33a)) instead of using Eq. (42a). This practice maintains the fourth-order accuracy as well as the dispersion level of the scheme. In order to obtain low numerical dispersion, consistent with the DRP scheme, it has been found that it is essential to treat the flux balance in the low-dispersion form (Eq. (42b)), but that this is not necessary for the high-order cell volume. This is even the case for non-uniform, curvilinear grids as the results of Section 5.1 will show.

As the vertices of the control volume Ω^{2h} do not lie at grid points but at cell centres (see Fig. 3), the coordinates of the cell centres are required to compute the area vectors of this control volume. To maintain the fourth-order accuracy of the scheme, these coordinates must be computed with fourth-order accuracy as well.

4.2. Numerical dispersion and implicit filtering

How relevant is it for LES to use a numerical scheme with low dispersion? As the subgrid-scale stresses are responsible for dissipating the structures with wave lengths close to the filter width, one would say that in the first place a numerical scheme should have low numerical dissipation. An alternative way of looking at the SGS stresses and the numerical errors is in terms of filtering. The SGS stresses are the result of applying a filter to the flow equations. The discretization of a spatial derivative can be written as the continuous derivative of a filtered variable [42,43]; in other words, discretization introduces an implicit filter and discretization errors can be seen as the effect of this implicit numerical filter. Minimizing the discretization errors relative to the SGS stresses therefore implies minimizing this implicit numerical filter relative to the explicit filter. This section will show that minimizing the implicit filter is equivalent to minimizing the numerical dispersion.

Following a recent analysis by Geurts [42], the second-order central discretization of the first derivative can be written as

$$\delta_h^{(2)} u = \frac{u(x+h)-u(x-h)}{2h} = \frac{\partial}{\partial x}\int_{x-h}^{x+h} \frac{u(s)}{2h}\mathrm{d}s = \frac{\partial}{\partial x}\int_{-\infty}^{\infty} G^{2h}(s)u(x-s)\mathrm{d}s, \tag{47}$$

with G^{Δ} the kernel function of the top-hat filter with filter width Δ. A central discretization based on Richardson extrapolation, such as the DRP scheme, consists of a combination of second-order central stencils,

$$\delta_h u = 2a_1\delta_h^{(2)}u + 4a_2\delta_{2h}^{(2)}u + 6a_3\delta_{3h}^{(2)}u, \tag{48}$$

so that it can also be written in terms of the top-hat filter as

$$\delta_h u = \frac{\partial}{\partial x}\int_{-\infty}^{\infty} G(s)u(x-s)\mathrm{d}s, \tag{49}$$

with the kernel function

$$G = 2a_1G^{2h} + 4a_2G^{4h} + 6a_3G^{6h}. \tag{50}$$

Taking the Fourier transform $\mathcal{F}_k$ of Eq. (49), with $\hat{u}_k = \mathcal{F}_k(u)$ and k the wave number (or substituting a mode $u = \hat{u}_k e^{ikx}$), turns the convolution into a product, so that

$$\mathcal{F}_k(\delta_h u) = \mathrm{i}k\hat{G}_k\hat{u}_k = \hat{G}_k\mathcal{F}_k\left(\frac{\partial u}{\partial x}\right), \tag{51}$$

with the transfer function of the implicit filter $\hat{G}_k$ given by

$$\hat{G}_k = 2a_1\hat{G}_k^{2h} + 4a_2\hat{G}_k^{4h} + 6a_3\hat{G}_k^{6h}. \tag{52}$$

where $\widehat{G}_k^{\Delta} = 2/(k\Delta)\sin(k\Delta/2)$ is the transfer function of the top-hat filter.

In the DRP scheme, the coefficients a_i have been optimized such that the Fourier symbol of the discrete derivative resembles as closely as possible the Fourier symbol of the continuous derivative over a wide range of wave numbers kh in the computational space. In this way, the dispersion-relation is preserved or, in other words, the numerical dispersion is minimized. Eq. (51) shows that the transfer function $\widehat{G}_k$ is the ratio of the Fourier symbols of the discrete and continuous derivatives. It follows that, for the DRP scheme, this transfer function will be close to one over a wide range of wave numbers, which means that the implicit filter has been minimized. Thus, minimizing dispersion is equivalent to minimizing the implicit filter.

The implicit filter of the DRP scheme is compared to the standard second, fourth, and sixth-order schemes in Fig. 4(a). Clearly, the DRP scheme has the weakest implicit filter, with the transfer function staying close to one up to $kh \approx 1$, i.e., with only about six grid cells per wave length. Fig. 4(b) compares the implicit filters of the DRP scheme and the standard second-order scheme to a reference top-hat filter with filter width Δ, varying the mesh size h relative to this filter width. For $h \geqslant \Delta/2$, the implicit filter of the second-order scheme is at least as strong as the reference filter. In contrast, for the DRP scheme, the implicit filter is already weaker than the reference filter with $h = \Delta$ for wave numbers up to $kh \approx 2$, i.e., with only about three grid cells (or filter widths) per wave length. Reducing the mesh size, the transfer function of the DRP scheme rapidly approaches the identity.

Comparing the implicit filters of the numerical schemes to a reference top-hat filter only serves as an illustration. For most hybrid RANS–LES models, the SGS model does not involve a filter explicitly. The SGS model is only assumed to model the SGS stresses obtained by applying some filter to the flow equations. It can be shown, however, that eddy-viscosity models, which are used almost exclusively in hybrid RANS–LES models, are only consistent with second-order filters [44]. Thus, comparing to a top-hat filter is more relevant than comparing to, for example, a cut-off filter.

4.3. Artificial diffusion

The high-order scheme defined so far has no numerical dissipation, due to the central, symmetric stencil and the skew-symmetric discretization. Nonetheless, this scheme is found to be stable for elementary test cases, typically using periodic boundary conditions, such as the convection of an isentropic vortex in a uniform flow, even on non-uniform grids (see Section 5.1). This can be attributed to the skew-symmetric discretization leading to the conservation by convection of kinetic (and internal) energy. For compressible flow, however, stability of the numerical scheme cannot be strictly proven (contrary to incompressible flow), as discussed at the end of Section 2.2. Therefore, sixth-order artificial diffusion is added, as an option, to the discretized equations in conservative form. When the second-order backward scheme is used for the time-integration, some numerical dissipation is also needed to obtain convergence for the multi-grid scheme used to solve the implicit system of equations per time step, in particular in inviscid regions of the flow. The impact of the artificial diffusion is assessed in Section 5. The artificial-diffusive flux balance is given by

$$B^a_{\mathbf{i}} = F^a_{i+1/2,j,k} - F^a_{i-1/2,j,k} + F^a_{ij+1/2,k} - F^a_{ij-1/2,k} + F^a_{ij,k+1/2} - F^a_{ij,k-1/2}. \tag{53}$$

In each of the discretized flow equations in divergence form (Eqs. (21), (22a), and (24)), this flux balance is subtracted from the flux balance $B^\beta_{\mathbf{i}}$ (Eq. (42b)) used for the convective terms in the flow equations. The fluxes consist of fifth-order differences of the flow variables:

$$F^a_{i+1/2,j,k} = \frac{k^{(6)}}{256}\lambda_{i+1/2,j,k}\left(U_{i+3,j,k} - 5U_{i+2,j,k} + 10U_{i+1,j,k} - 10U_{i,j,k} + 5U_{i-1,j,k} - U_{i-2,j,k}\right), \tag{54}$$

with U the relevant flow variable ($\rho, \rho\boldsymbol{u}$, or ρE), and are scaled by the spectral radius of the flux Jacobian λ,

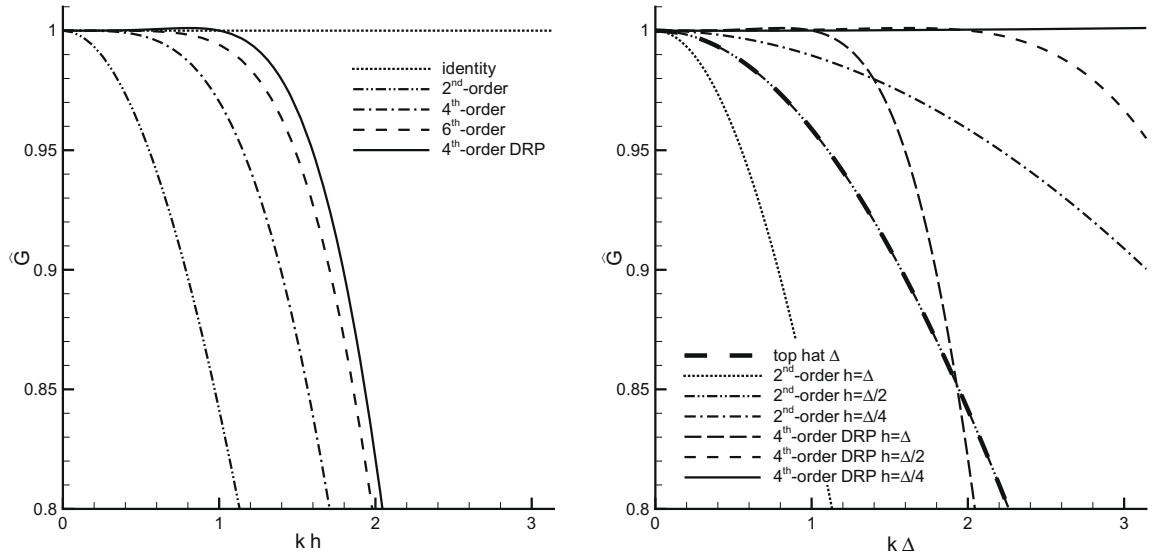

(a) Transfer functions plotted against wave number k times mesh width h

(b) Transfer functions for different mesh sizes compared to top-hat filter with filter width Δ, plotted against wave number k times filter width Δ

Fig. 4. Transfer functions of the implicit filters of the DRP scheme and standard central differencing schemes.

$$\lambda = |\boldsymbol{u}\cdot\boldsymbol{A}^h| + c\|\boldsymbol{A}^h\|_2. \tag{55}$$

with $\|.\|_2$ the Euclidean norm. This form of artificial diffusion introduces a discretization error of fifth order, leaving the fourth-order accuracy of the scheme intact. The parameter $k^{(6)}$ is typically taken equal to $k^{(6)} = 2$ when using second-order backward time-integration. Note that the seven-point stencil of the total scheme is maintained.

5. Results

5.1. Convection of an isentropic vortex

In order to test the capability of the high-order finite-volume scheme to accurately capture vortices without significant dissipation or dispersion, the convection of a 2D isentropic vortex in a uniform flow is considered. The uniform flow is in the positive x direction at a Mach number $M_\infty = 0.5$. The initial solution is given by

$$\boldsymbol{u} = \begin{pmatrix} u_\infty \\ 0 \end{pmatrix} + u_A \mathrm{e}^{(1-(r/b)^2)/2} \begin{pmatrix} (y-y_0)/b \\ -(x-x_0)/b \end{pmatrix}, \tag{56}$$

and

$$\frac{T}{T_\infty} = \left(\frac{p}{p_\infty}\right)^{(\gamma-1)/\gamma} = \left(\frac{\rho}{\rho_\infty}\right)^{\gamma-1} = 1 - \frac{\gamma-1}{2}\frac{u_A^2}{c_\infty^2}\mathrm{e}^{1-(r/b)^2}, \tag{57}$$

with T the temperature, with $r^2 = (x-x_0)^2 + (y-y_0)^2$ the distance from the vortex centre (x_0,y_0), and with b the radius where the velocity induced by the vortex reaches its maximum value u_A. The exact solution of the compressible Euler equations simply consists of a translation of the vortex by a distance equal to the mean-flow velocity times the time interval. The flow domain is defined as $\boldsymbol{x} \in [-25L, 25L]^2$ with periodic boundary conditions, where $L = \sqrt{\ln 2}\, b$ is a representative length scale of the vortex (with $\mathrm{e}^{-(r/b)^2} = \frac{1}{2}$ at $r = L$).

A strong vortex is considered with $u_A/u_\infty = 0.8$. It is initially located at $(x_0,y_0) = (-18.75L, 0)$ and convected for a time period $u_\infty t/L = 37.5$ to end up at the location $(x,y) = (18.75L, 0)$. Computations are performed on a strongly non-uniform grid, with strong stretching and skewness, as illustrated in Fig. 5. The grid has been obtained by smoothly mapping a uniform grid from the computational domain to the physical domain. The number of cells is varied from 100×100 to 400×400. The equations are integrated in time by a low-storage 4-stage Runge–Kutta scheme. As this time-integration method is only second-order accurate for non-linear equations, the time step is taken proportional to the square of the mesh size in the computational domain, so that the time-integration error is of fourth-order in the mesh size. On the coarsest grid, a time step $u_\infty \Delta t/L = \frac{1}{18}$ is used.

The second-order scheme, the basic fourth-order scheme, and the low-dispersion fourth-order scheme are used. For all three schemes, computations using the particular divergence form of the convective operator (Eq. (20)) that is equivalent to the skew-symmetric form (Eq. (17)) are compared to computations based on a standard divergence form that is not equivalent to the skew-symmetric form. Thus, in total six different schemes are considered. For this case, the skew-symmetric form is stable without artificial diffusion even on this non-uniform grid. For the non-symmetric divergence form, standard flux averaging (using $\boldsymbol{F} = \overline{\rho\boldsymbol{u}}\overline{\phi}$ in Eq. (16)) turned out to be unstable. Therefore, in the non-symmetric divergence form, the fluxes at the cell faces are computed by averaging the flow variables per unit volume as in the Jameson-type scheme ($\boldsymbol{F} = \overline{\rho\boldsymbol{u}}\overline{\rho\phi}/\overline{\rho}$), which differs only slightly from the skew-symmetric form (see the end of Section 3.1).

Fig. 6 shows the temperature distributions on the medium grid (200×200 cells) computed with all six schemes. For the non-symmetric second-order scheme, the vortex has clearly lost its shape, while also the centre of the vortex has drifted to a

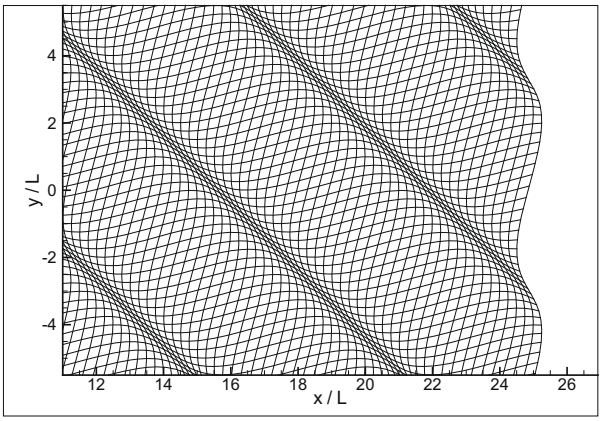

Fig. 5. Strongly non-uniform grid (200×200 cells) used for convection of strong isentropic vortex (detail around location $(18.75L, 0)$).

positive y position (of approximately $y = L$). Using the skew-symmetric form, the shape of the vortex is better preserved than using the non-symmetric divergence form (in particular visible for the second-order and basic fourth-order schemes). The low-dispersion fourth-order scheme is the most successful in maintaining the shape and position of the vortex. Note that the vortex consists of a collection of waves with different wave lengths. Loss of shape and position can be interpreted as the result of these waves travelling at different speeds, i.e., the result of numerical dispersion. Thus, these results show that the low-dispersion finite-volume method defined here truly has low dispersion for non-linear flow equations on a strongly non-uniform grid.

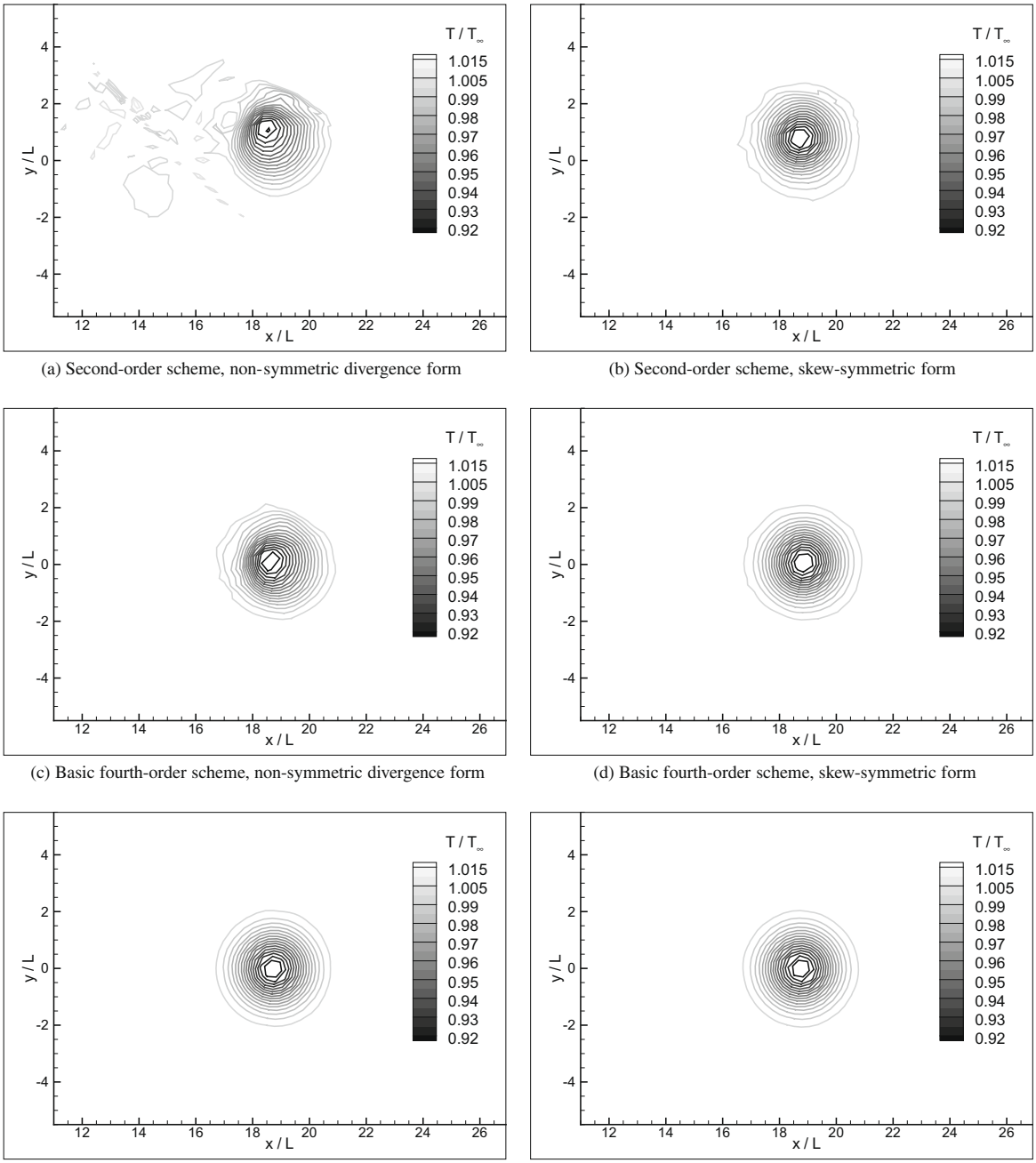

(a) Second-order scheme, non-symmetric divergence form

(b) Second-order scheme, skew-symmetric form

(c) Basic fourth-order scheme, non-symmetric divergence form

(d) Basic fourth-order scheme, skew-symmetric form

(e) Low-dispersion fourth-order scheme, non-symmetric divergence form

(f) Low-dispersion fourth-order scheme, skew-symmetric form

Fig. 6. Convection of strong isentropic vortex on strongly non-uniform grid: temperature field at time $u_\infty t/L = 37.5$ (centre should be located at $(x,y) = (18.75L, 0)$) on medium grid (200×200 cells).

Fig. 7 gives the difference of the numerical solution with the analytical solution as a function of the grid resolution for all six schemes (with h the mesh size in the computational domain). This shows that the fourth-order schemes are indeed fourth-order accurate on this strongly non-uniform, curvilinear grid. For the low-dispersion scheme, the error is reduced by an order of magnitude compared to the basic fourth-order scheme.

As the chosen approach for the non-symmetric divergence form differs only slightly from the skew-symmetric form, one would not expect large differences in the error levels. Indeed, the error levels for the velocity components are indiscernible. For the entropy, however, a clear reduction of the error by almost an order of magnitude is seen for the skew-symmetric form (Fig. 7(d)). Essentially, there is less entropy production using the skew-symmetric form, because it ensures that there is no dissipation (or creation) of kinetic energy stemming from the discretized convective operator. Larger differences may be expected if the non-symmetric divergence form would be based on averaging the fluxes, since it requires artificial diffusion to maintain stability.

Although the present computations are stable without artificial diffusion, the effect of including sixth-order artificial diffusion is also assessed. Only the fourth-order low-dispersion skew-symmetric scheme is considered. As this scheme has the highest accuracy, the effect of artificial diffusion will be the most pronounced. Fig. 8 compares the errors as a function of the mesh size for the computations with and without artificial diffusion. Two levels of artificial diffusion are considered: $k^{(6)} = 0.5$ and $k^{(6)} = 2$. As expected, the fourth-order accuracy is maintained. Comparing Fig. 8(a) to 7(a) (error in velocity)

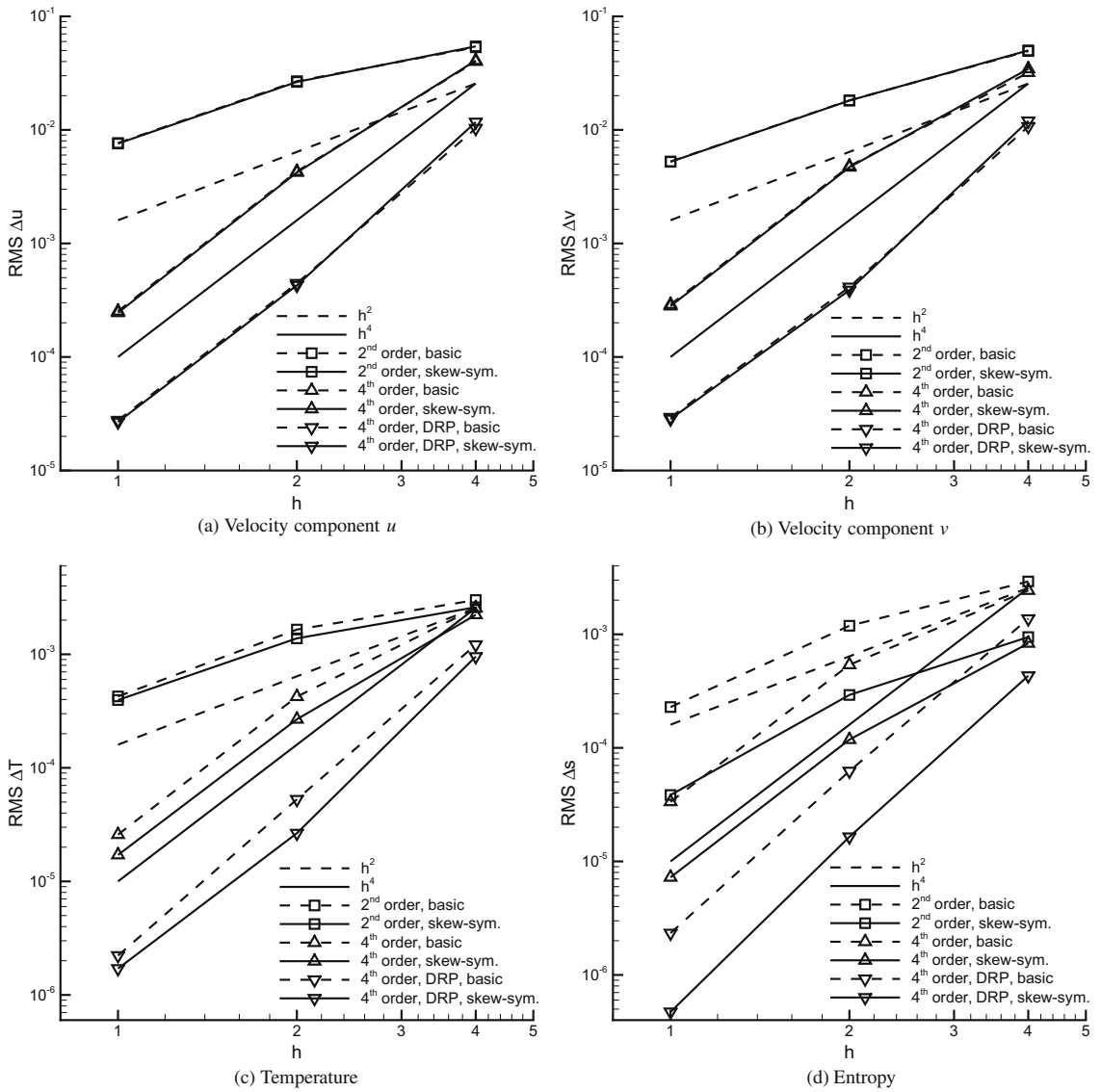

(a) Velocity component u

(b) Velocity component v

(c) Temperature

(d) Entropy

Fig. 7. Convection of strong isentropic vortex on strongly non-uniform grid: grid dependence of root-mean-square value of difference with analytical solution at time $u_\infty t/L = 37.5$.

shows that the low-dispersion scheme with artificial diffusion is still substantially more accurate than the basic fourth-order scheme without artificial diffusion. In particular, using a coefficient of $k^{(6)} = 0.5$ does not substantially increase the error level. Comparing Fig. 8(b) to 7(d), however, shows that the error level in entropy is substantially increased by the artificial diffusion. Essentially, the gain in accuracy due to the skew-symmetric form is lost. This was to be expected, as the numerical diffusion reintroduces numerical dissipation of kinetic energy that had been removed by the skew-symmetric form.

For the present inviscid computations, the computational costs of the different schemes have been determined in terms of the CPU time on the finest grid level, using a single processor of the NEC SX-8. Using the skew-symmetric form instead of a standard divergence form increases the costs by a factor 1.3, using the basic fourth-order instead of second-order scheme by a factor 1.8, and using the low-dispersion instead of the basic fourth-order scheme by a factor 1.2. Thus, in total, the low-dispersion fourth-order skew-symmetric scheme is a factor 2.8 more expensive than the basic second-order scheme using a standard divergence form. For the fourth-order and low-dispersion schemes, the increased numerical accuracy clearly outweighs the increased computational costs. To obtain the same accuracy as the second-order scheme on the finest grid level, the fourth-order scheme allows the mesh size to be at least twice as large and the low-dispersion fourth-order scheme three to four times as large. In 3D, this means that the low-dispersion fourth-order skew-symmetric scheme is a factor 10–20 cheaper than the basic second-order scheme (keeping the same size for the time step). Whether one considers the (small) increase of computational cost for the skew-symmetric form worthwhile, depends on the relevance of the reduced entropy error and the improved numerical stability.

5.2. Decaying isotropic homogeneous turbulence

The high-order finite-volume scheme is intended to be used for the LES regions of hybrid RANS–LES computations. To assess the numerical scheme in pure LES mode, the decay of isotropic homogeneous turbulence is considered. The results are compared to the experiment of Comte-Bellot and Corrsin [45]. In this experiment, the turbulence was generated by a grid with mesh size $M_g = 5.08$ cm and with an onset velocity of $U_0 = 10$ m/s. The Reynolds number based on these scales is $Re_0 = U_0 M_g/\nu = 34{,}000$. In the computations, a cubic box of thickness $L = 10M_g$ is used with periodic boundary conditions. The initial solution consists of a random velocity field generated from the filtered experimental energy spectrum at time $t^+ = t\, U_0/M_g = 42$.

X-LES computations with the second-order scheme have been presented before [8]. The same computational procedure is followed here. To study the grid dependence of the numerical scheme, a fixed filter width $\Delta = L/32$ is employed, while the mesh size is varied from $h = \Delta$ to $h = \Delta/4$. Because LES computes a filtered velocity field, the experimental data is filtered with the top-hat filter to allow a proper comparison (see [8] for details).

In Large-Eddy Simulations, numerical errors stemming mainly from the convection terms may interfere with the subgrid-scale model, especially for second-order methods. The high-order scheme has been developed to reduce those numerical errors in particular. Thus, for X-LES computations with the high-order scheme, only the inviscid terms of the basic flow equations are discretized with high order. The viscous terms and the Reynolds and SGS stresses are discretized with a standard second-order central scheme. Also, the k and ω equations are discretized with a second-order scheme [46].

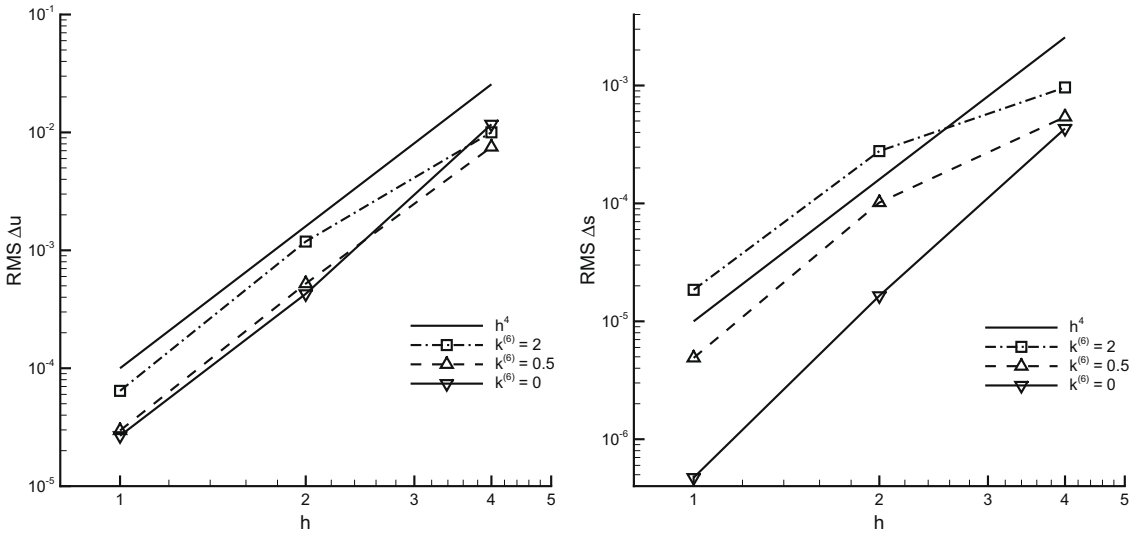

(a) Velocity component u (b) Entropy

Fig. 8. Convection of strong isentropic vortex on strongly non-uniform grid: grid dependence of root-mean-square value of difference with analytical solution at time $u_\infty t/L = 37.5$ of fourth-order low-dispersion skew-symmetric scheme with and without artificial diffusion.

For compressible flow, the skew-symmetric form ensures that the kinetic energy is conserved by the convective operator. This is illustrated by first performing inviscid computations of homogeneous turbulence at compressible flow conditions (Mach number $M_1 = 0.2$ based on the initial turbulence intensity $u_1 = 0.222$ m/s). Without viscous dissipation, the total kinetic energy in the box can only change due to the work done by the pressure. Fig. 9 gives the time dependence of the total kinetic energy for computations on the coarse grid ($h = \Delta$) with the low-dispersion fourth-order scheme without artificial diffusion. Both the skew-symmetric form and the non-symmetric divergence form (using flux averaging) are considered. The low-storage 4-stage Runge–Kutta scheme has been used with a small time step ($\Delta t^+ = 0.873$ or $u_1 \Delta t/h = 0.062$). The computation with the non-symmetric divergence form shows a rapid increase of the total kinetic energy and breaks down within a short time period. Clearly, due to the lack of energy conservation, this method is unstable. For the computation with the skew-symmetric form, the stability is strongly enhanced and the total kinetic energy is practically constant on the time scale shown, because there is no numerical production or dissipation of kinetic energy originating from the discretized convective terms in the momentum equation. Therefore, for X-LES computations, the decay of the total kinetic energy will be determined by the SGS model and not by numerical dissipation.

Next, the grid convergence is considered for X-LES computations in pure LES mode, i.e., using a k-equation SGS model, at incompressible flow conditions. The equations are integrated in time by a second-order implicit scheme with time step $\Delta t^+ = 3.49$. Fig. 10 shows the grid dependence of the energy spectra at times $t^+ = 98$ and $t^+ = 171$ for the second-order scheme with fourth-order artificial diffusion and the skew-symmetric low-dispersion fourth-order scheme with sixth-order artificial diffusion. The level of artificial diffusion is such that the damping at the highest wave numbers (point-to-point oscillations) is the same for both schemes ($k^{(6)} = 2$ for the sixth-order artificial diffusion). This ensures that the multi-grid scheme used to solve the implicit system of equations per time step shows the same convergence rate for both schemes. The fourth-order scheme has clearly improved the grid convergence over the second-order scheme. For sufficient accuracy, the second-order scheme requires at least a mesh size of $h = \Delta/4$, i.e., four cells per filter width, while the fourth-order scheme obtains the same level of accuracy with a mesh size of $h = \Delta/2$, i.e., two cells per filter width.

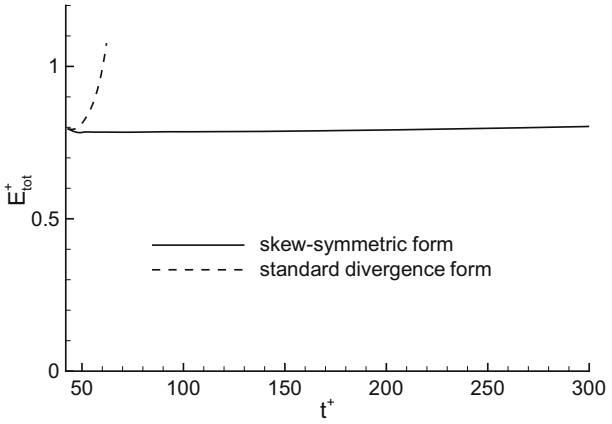

Fig. 9. Compressible isotropic homogeneous turbulence: time dependence of total kinetic energy for inviscid computations with low-dispersion fourth-order schemes without artificial diffusion using skew-symmetric and standard divergence forms.

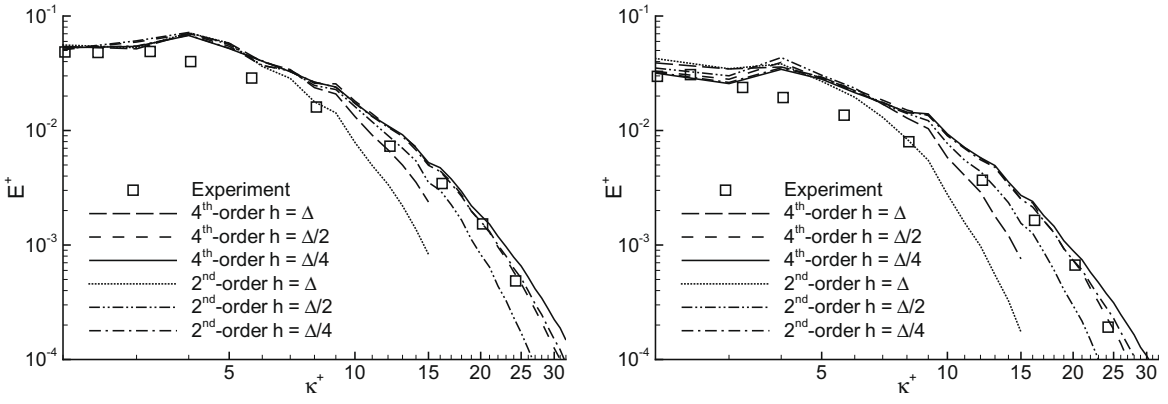

(a) Time $t^+ = 98$ (b) Time $t^+ = 171$

Fig. 10. Incompressible isotropic homogeneous turbulence: grid dependence of energy spectra for second-order and low-dispersion fourth-order schemes.

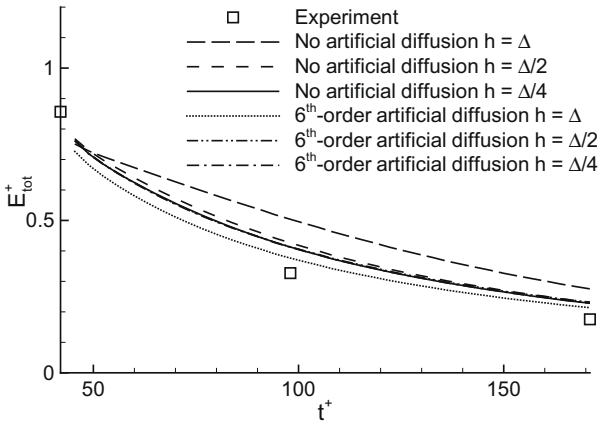

Fig. 11. Incompressible isotropic homogeneous turbulence: decay of total kinetic energy for low-dispersion fourth-order scheme with and without sixth-order artificial diffusion.

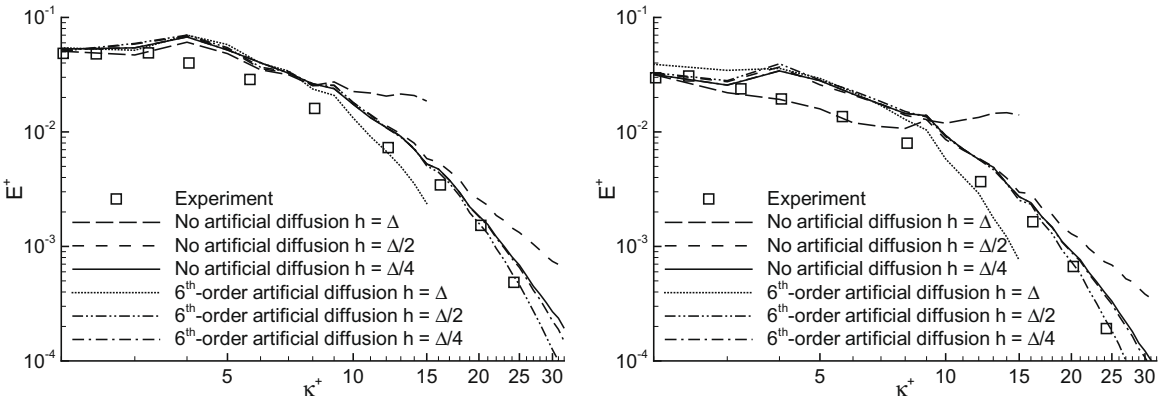

(a) Time $t^+ = 98$ (b) Time $t^+ = 171$

Fig. 12. Incompressible isotropic homogeneous turbulence: grid dependence of energy spectra for low-dispersion fourth-order scheme with and without sixth-order artificial diffusion.

For the present computations, artificial diffusion is not needed to maintain stability. As explained in Section 4.3, however, there may be practical reasons to include some artificial diffusion. Therefore, the effect of artificial diffusion on the numerical accuracy is considered. Fig. 11 shows the decay of the total kinetic energy for the fourth-order low-dispersion skew-symmetric scheme with and without sixth-order artificial diffusion. Fig. 12 shows the grid dependence of the energy spectra with and without artificial diffusion. The decay of kinetic energy is virtually grid-independent at a mesh size $h = \Delta/2$. The grid-converged solution is purely determined by the SGS model, not by numerical errors. The computations with and without artificial diffusion converge towards this solution from opposite sides, but with similar convergence rates. Thus, at least for this case, the numerical errors introduced by a limited amount of sixth-order artificial diffusion are of the same order as the other numerical errors. Artificial diffusion is not needed, however, to obtain a grid-converged solution purely determined by the SGS model.

For these LES computations, the increase in computational cost for the high-order scheme is only a factor 1.4. The viscous and SGS terms as well as the k and ω equations make the computations more expensive than inviscid computations, thus reducing the relative cost of the high-order scheme. The additional cost of the skew-symmetric form is now effectively negligible.

6. Conclusion

A high-order finite-volume method with low numerical dissipation and dispersion has been developed for the compressible flow equations such that the mathematical skew symmetry of convection is preserved. It has been shown that both momentum and kinetic energy, as well as sound-velocity and internal energy, are locally conserved by convection, in a discrete sense, even on non-uniform, curvilinear grids. Furthermore, the method is strictly fourth-order accurate on such grids,

while maintaining the conservation properties. The skew symmetry prevents spurious production or dissipation of kinetic energy, which could interfere with a subgrid-scale model. The skew symmetry has been preserved by combining second-order methods using Richardson extrapolation and by using constant coefficients for the discretization stencil, even on non-uniform grids. By using three instead of two control volumes in the Richardson extrapolation, an additional degree of freedom is introduced that allows the minimization of numerical dispersion.

A grid convergence study for the convection of an isentropic vortex has confirmed that the method is fourth-order accurate on smooth, strongly non-uniform, curvilinear grids. For this study, the low-dispersion approach reduces the errors in all variables by an order of magnitude and the skew-symmetry preservation reduces the entropy error by an additional order of magnitude, compared to a basic fourth-order method.

Finally, the decay of homogeneous isotropic turbulence has been computed. In the compressible, inviscid case, using the discrete skew-symmetric form enhances the numerical stability in the sense that the total kinetic energy has only a very weak growth rate compared to a computation using a standard discrete divergence form of convection. For Large-Eddy Simulations, a grid convergence study has shown that the fourth-order solution with a mesh size equal to half the filter width is comparable to the second-order solution with a mesh size equal to a quarter of the filter width. In other words, the mesh size can be twice as large for the new fourth-order method to obtain the same numerical accuracy, reducing the computational effort by a factor eight in 3D.

Acknowledgment

This work is performed within the NLR Programme 'Kennis als Vermogen, Platformtechnology and Flight Physics'. Some results were obtained within the EU project DESider (Detached Eddy Simulation for Industrial Aerodynamics), which is funded by the European Union under Contract No. AST3-CT-2003-502842 of the European Commission.

The author would like to thank Prof. Arthur Veldman for fruitful discussions on skew symmetry and high-order methods.

Appendix A. Detailed derivations

The rules of Eq. (15) are derived in detail here. Without loss of generality, let face f be the face between cells $\Omega_{i,j,k}$ and $\Omega_{i+1,j,k}$. Rule (15a) is derived as follows:

$$\widetilde{(uv)}_f v_f = \frac{1}{2}\left((uv)_{i,j,k} v_{i+1,j,k} + (uv)_{i+1,j,k} v_{i,j,k}\right) = \frac{1}{2}\left(u_{i,j,k} + u_{i+1,j,k}\right) v_{i,j,k} v_{i+1,j,k} = \bar{u}_f \widetilde{v v}_f. \tag{A.1}$$

Rule (15b) is derived as follows:

$$\begin{aligned}\bar{u}_f \bar{v}_f &= \frac{1}{2}\left(u_{i,j,k} + u_{i+1,j,k}\right)\frac{1}{2}\left(v_{i,j,k} + v_{i+1,j,k}\right) = \frac{1}{4}\left(u_{i,j,k} v_{i,j,k} + u_{i+1,j,k} v_{i+1,j,k}\right) + \frac{1}{4}\left(u_{i,j,k} v_{i+1,j,k} + u_{i+1,j,k} v_{i,j,k}\right)\\ &= \frac{1}{2}\overline{uv}_f + \frac{1}{2}\widetilde{uv}_f,\end{aligned} \tag{A.2}$$

so that summing over all faces f of cell $\Omega_{\boldsymbol{i}}$ gives

$$\nabla_{\boldsymbol{i}} \bar{u}\bar{v} = \frac{1}{2}\nabla_{\boldsymbol{i}} \overline{uv} + \frac{1}{2}\nabla_{\boldsymbol{i}} \widetilde{uv}, \tag{A.3}$$

Finally, rule (15c) is derived as follows:

$$\begin{aligned}\widetilde{uv}_f &= \frac{1}{2}\left(u_{i,j,k} v_{i+1,j,k} + u_{i+1,j,k} v_{i,j,k}\right) = u_{i,j,k}\frac{1}{2}\left(v_{i,j,k} + v_{i+1,j,k}\right) + v_{i,j,k}\frac{1}{2}\left(u_{i,j,k} + u_{i+1,j,k}\right) - u_{i,j,k} v_{i,j,k}\\ &= u_{i,j,k}\bar{v}_f + v_{i,j,k}\bar{u}_f - u_{i,j,k} v_{i,j,k},\end{aligned} \tag{A.4}$$

so that summing over all faces f of cell $\Omega_{\boldsymbol{i}}$ gives

$$\nabla_{\boldsymbol{i}} \widetilde{uv} = u_{\boldsymbol{i}} \nabla_{\boldsymbol{i}} \bar{v} + v_{\boldsymbol{i}} \nabla_{\boldsymbol{i}} \bar{u} - u_{\boldsymbol{i}} v_{\boldsymbol{i}} \frac{1}{V_{\boldsymbol{i}}} \sum_f \boldsymbol{A}_f = u_{\boldsymbol{i}} \nabla_{\boldsymbol{i}} \bar{v} + v_{\boldsymbol{i}} \nabla_{\boldsymbol{i}} \bar{u}, \tag{A.5}$$

where the geometric conservation law (Eq. (13)) has been used.

Appendix B. Time-integration method preserving skew symmetry

In this appendix, a time-integration method is sought that preserves the skew symmetry of the compressible convection operator. For incompressible flow, two approaches have been considered by Verstappen and Veldman [17]: the midpoint rule and the leapfrog method. Both schemes are also considered here for compressible flows. For incompressible flows, preservation of skew symmetry results, for both schemes, in a conservative discretization of the kinetic energy equation. Only for the midpoint rule, however, does this imply that a discrete energy norm cannot increase.

To preserve skew symmetry for a time-integration method, Eq. (18) should also hold with a discretized time derivative. One approach consists of discretizing the time derivative in the same manner as the spatial gradient,

$$\mathrm{d}_t^n \phi = \frac{\phi^{n+1/2} - \phi^{n-1/2}}{\Delta t}, \tag{B.1}$$

with superscript n indicating the time level and with Δt the time-step size. Averaging towards time level $n+1/2$ is defined analogous to Eq. (14) and equivalents of relations (15) also hold for the discrete time derivative. Discretizing the skew-symmetric form both in space and time as

$$K_{\boldsymbol{i}}^n \phi = \frac{1}{2}\mathrm{d}_t^n \overline{\rho_{\boldsymbol{i}}\phi_{\boldsymbol{i}}} + \frac{1}{2}\rho_{\boldsymbol{i}}^n \mathrm{d}_t^n \overline{\phi_{\boldsymbol{i}}} + \frac{1}{2}\nabla_{\boldsymbol{i}} \cdot \overline{\rho^n \boldsymbol{u}^n \phi^n} + \frac{1}{2}\rho_{\boldsymbol{i}}^n \boldsymbol{u}_{\boldsymbol{i}}^n \cdot \nabla_{\boldsymbol{i}} \bar{\phi}^n, \tag{B.2}$$

one finds the following conservative discretization for the divergence form applied to ϕ^2,

$$\phi_{\boldsymbol{i}}^n K_{\boldsymbol{i}}^n \phi = \mathrm{d}_t^n \left(\overline{\rho_{\boldsymbol{i}}} \frac{1}{2} \widetilde{\phi_{\boldsymbol{i}}\phi_{\boldsymbol{i}}} \right) + \nabla_{\boldsymbol{i}} \cdot \left(\overline{\rho^n \boldsymbol{u}^n} \frac{1}{2} \widetilde{\phi^n \phi^n} \right), \tag{B.3}$$

with $\widetilde{\phi_{\boldsymbol{i}}\phi_{\boldsymbol{i}}} = \phi_{\boldsymbol{i}}^n \phi_{\boldsymbol{i}}^{n+1}$. The time derivative, however, contains a term which is not strictly quadratic. Integrating this equation over the flow domain leads to conservation of $\phi^n \phi^{n+1}$ rather than ϕ^2, and the integral of this product is not strictly an energy norm. Furthermore, this time discretization is essentially the leapfrog method, which requires further modifications to be stable when including diffusion [47].

An alternative approach for the time-integration is the midpoint rule, which does lead to a conservative discretization involving a true energy norm for incompressible flow [17]. Discretize the time derivative at time level $n+1/2$ as

$$\mathrm{d}_t^{n+1/2} \phi = \frac{\phi^{n+1} - \phi^n}{\Delta t}. \tag{B.4}$$

The following discrete product rule can be derived,

$$\mathrm{d}_t^{n+1/2}(uv) = u^{n+1/2} \mathrm{d}_t^{n+1/2} v + v^{n+1/2} \mathrm{d}_t^{n+1/2} u, \tag{B.5}$$

with $u^{n+1/2} = \frac{1}{2}(u^{n+1} + u^n)$. If the skew-symmetric form is now discretized both in space and time as

$$K_{\boldsymbol{i}}^{n+1/2} \phi = \frac{1}{2}\mathrm{d}_t^{n+1/2}(\rho_{\boldsymbol{i}}\phi_{\boldsymbol{i}}) + \frac{1}{2}\rho_{\boldsymbol{i}}^{n+1/2} \mathrm{d}_t^{n+1/2}\phi_{\boldsymbol{i}} + \frac{1}{2}\nabla_{\boldsymbol{i}} \cdot \overline{(\rho \boldsymbol{u})^{n+1/2} \phi^{n+1/2}} + \frac{1}{2}(\rho \boldsymbol{u})_{\boldsymbol{i}}^{n+1/2} \cdot \nabla_{\boldsymbol{i}} \overline{\phi^{n+1/2}}, \tag{B.6}$$

then the following discretization for the divergence form applied to ϕ^2 is found,

$$\phi_{\boldsymbol{i}}^{n+1/2} K_{\boldsymbol{i}}^{n+1/2} \phi = \mathrm{d}_t^{n+1/2} \left(\rho_{\boldsymbol{i}} \frac{1}{2} \phi_{\boldsymbol{i}}^2 \right) + \nabla_{\boldsymbol{i}} \cdot \left(\overline{(\rho \boldsymbol{u})^{n+1/2}} \frac{1}{2} \widetilde{\phi^{n+1/2} \phi^{n+1/2}} \right) + \frac{1}{2} \left(\rho_{\boldsymbol{i}}^{n+1/2} \phi_{\boldsymbol{i}}^{n+1/2} - (\rho\phi)_{\boldsymbol{i}}^{n+1/2} \right) \mathrm{d}_t^{n+1/2} \phi_{\boldsymbol{i}}. \tag{B.7}$$

Although now the equation includes the time derivative of a truly quadratic form, there is an additional non-conservative term that only disappears if the density is constant. Thus, this approach also does not lead to a suitable symmetry-preserving time-integration method for compressible flow.

References

[1] P.R. Spalart, W.-H. Jou, M. Strelets, S.R. Allmaras, Comments on the feasibility of LES for wings, and on a hybrid RANS/LES approach, in: C. Liu, Z. Liu (Eds.), Advances in DNS/LES, Proc. 1st AFOSR Int. Conf. on DNS/LES, 1997, Ruston (LA), USA Greyden Press, 1997.
[2] S. Ghosal, Mathematical and physical constraints on large-eddy simulation of turbulence, AIAA J. 37 (4) (1999) 425–433.
[3] A.G. Kravchenko, P. Moin, On the effect of numerical errors in large eddy simulations of turbulent flows, J. Comput. Phys. 131 (1997) 310–322.
[4] B. Vreman, B. Geurts, H. Kuerten, Comparison of numerical schemes in large eddy simulation of the temporal mixing layer, Int. J. Numer. Meth. Fluids 2 (1996) 297–311.
[5] J. Meyers, B.J. Geurts, M. Baelmans, Database analysis of errors in large eddy simulation, Phys. Fluids 15 (2003) 2740–2755.
[6] C. Fureby, F.F. Grinstein, Monotonically integrated large eddy simulation of free shear flows, AIAA J. 37 (5) (1999) 544–556.
[7] J.C. Kok, A symmetry and dispersion-relation preserving high-order scheme for aeroacoustics and aerodynamics, in: ECCOMAS CFD 2006, Egmond aan Zee, The Netherlands, 2006, NLR-TP-2006-525.
[8] J.C. Kok, H.S. Dol, B. Oskam, H. van der Ven, Extra-large eddy simulation of massively separated flows, in: 42nd AIAA Aerospace Sciences Meeting, Reno (NV), USA, 2004, AIAA Paper 2004-264.
[9] J.C. Kok, B.I. Soemarwoto, H. van der Ven, Extra-large eddy simulations using a high-order finite-volume scheme, in: S.H. Peng, W. Haase (Eds.), Advances in Hybrid RANS–LES Modelling, Notes on Numerical Fluid Mechanics and Multidisciplinary Design, vol. 97, Springer, 2008, pp. 87–96. NLR-TP-2007-800.
[10] N.N. Mansour, P. Moin, W.C. Reynolds, J.H. Ferziger, Improved methods for large eddy simulations of turbulence, Turbulent Shear Flows 1 (1979) 386–401.
[11] G.A. Blaisdell, E.T. Spyropoulos, J.H. Qin, The effect of the formulation of nonlinear terms on aliasing errors in spectral methods, Appl. Numer. Math. 21 (3) (1996) 207–219.
[12] F.H. Harlow, J.E. Welch, Numerical calculations of time-dependent viscous incompressible flow with free surface, Phys. Fluids 8 (1965) 2182–2189.
[13] Y. Morinishi, T.S. Lund, O.V. Vasilyev, P. Moin, Fully conservative higher order finite difference schemes for incompressible flow, J. Comput. Phys. 143 (1998) 90–124.
[14] O.V. Vasilyev, High order finite difference schemes on non-uniform meshes with good conservation properties, J. Comput. Phys. 157 (2000) 746–761.
[15] R.W.C.P. Verstappen, A.E.P. Veldman, Direct numerical simulation of turbulence at lower costs, J. Eng. Math. 32 (1997) 143–159.
[16] R.W.C.P. Verstappen, A.E.P. Veldman, Spectro-consistent discretization of Navier–Stokes: a challenge to RANS and LES, J. Eng. Math. 34 (1998) 163–179.
[17] R.W.C.P. Verstappen, A.E.P. Veldman, Symmetry-preserving discretization of turbulent flow, J. Comput. Phys. 187 (1) (2003) 343–368.

[18] A.E.P. Veldman, K. Rinzema, Playing with nonuniform grids, J. Eng. Math. 26 (1992) 119–130.
[19] R.W.C.P. Verstappen, A.E.P. Veldman, Numerical simulation of a turbulent flow in a channel with surface mounted cubes, Appl. Sci. Res. 59 (1998) 395–408.
[20] W.J. Feiereisen, W.C. Reynolds, J.H. Ferziger, Numerical simulation of a compressible, homogeneous, turbulent shear flow, Report TF-13, Thermosciences Division, Mechanical Engineering, Stanford University, 1981.
[21] A.E. Honein, P. Moin, Higher entropy conservation and numerical stability of compressible turbulence simulations, J. Comput. Phys. 201 (2) (2004) 531–545.
[22] F. Ducros, F. Laporte, T. Souléres, V. Guinot, P. Moinat, B. Caruelle, High-order fluxes for conservative skew-symmetric-like schemes in structured meshes: application to compressible flows, J. Comput. Phys. 161 (2000) 14–139.
[23] C.A. Kennedy, A. Gruber, Reduced aliasing formulations of the convective terms within the Navier–Stokes equations for a compressible fluid, J. Comput. Phys. 227 (2008) 1676–1700.
[24] S. Nagarajan, S.K. Lele, J.H. Ferziger, A robust high-order compact method for large eddy simulation, J. Comput. Phys. 191 (2) (2003) 392–419.
[25] N. Park, J.Y. Yoo, H. Choi, Discretization errors in large eddy simulation: on the suitability of centered and upwind-biased compact difference schemes, J. Comput. Phys. 198 (2) (2004) 580–616.
[26] G. Rubio, M. Baelmans, W. Desmet, Finite volume convective flux reconstruction using high-order skew-symmetric-like schemes, in: 13th AIAA/CEAS Aeroacoustics Conference, Rome, Italy, 2007, AIAA Paper 2007-3407.
[27] C.K.W. Tam, J.C. Webb, Dispersion-relation-preserving finite difference schemes for computational acoustics, J. Comput. Phys. 107 (1993) 262–281.
[28] S.K. Lele, Compact finite difference schemes with spectral-like resolution, J. Comput. Phys. 103 (1) (1992) 16–42.
[29] M.R. Visbal, D.P. Rizzetta, Large-eddy simulation on curvilinear grids using compact differencing and filtering schemes, J. Fluids Eng. 124 (2002) 836–847.
[30] T. Colonius, S.K. Lele, Computational aeroacoustics: progress on nonlinear problems of sound generation, Prog. Aerosp. Sci. 40 (6) (2004) 345–416.
[31] M.R. Visbal, D.V. Gaitonde, On the use of high-order finite-difference schemes on curvilinear and deforming meshes, J. Comput. Phys. 181 (2002) 155–185.
[32] C. Lacor, S. Smirnov, M. Baelmans, A finite volume formulation of compact central schemes on arbitrary structured grids, J. Comput. Phys. 198 (2) (2004) 535–566.
[33] M. Piller, E. Stalio, Finite-volume compact schemes on staggered grids, J. Comput. Phys. 197 (1) (2004) 299–340.
[34] M. Piller, E. Stalio, Compact finite volume schemes on boundary-fitted grids, J. Comput. Phys. 227 (9) (2008) 4736–4762.
[35] M. Popescu, W. Shyy, M. Garbey, Finite volume treatment of dispersion-relation-preserving and optimized prefactored compact schemes for wave propagation, J. Comput. Phys. 210 (2) (2005) 705–729.
[36] S. Smirnov, C. Lacor, M. Baelmans, A finite-volume formulation for compact scheme with applications to LES, in: 15th AIAA Computational Fluid Dynamics Conference, Anaheim, CA, 2001, AIAA 2001-2546.
[37] D.V. Nance, K. Viswanathan, L.N. Sankar, Low-dispersion finite-volume scheme for aeroacoustic applications, AIAA J. 35 (2) (1997) 255–262.
[38] R. Courant, D. Hilbert, Methods of Mathematical Physics, vol. 2, Interscience Publishers, New York, 1962.
[39] E.T. Spyropoulos, G.A. Blaisdell, Evaluation of the dynamic model for simulations of compressible decaying isotropic turbulence, AIAA J. 34 (5) (1996) 990–998.
[40] A. Jameson, Numerical simulation of the Euler equations for compressible inviscid fluids, Report MAE 1643, Dept. of Mech. and Aerosp. Eng., Princeton University, 1985.
[41] C.K.W. Tam, Computational aeroacoustics: issues and methods, AIAA J. 33 (1995) 1788–1796.
[42] B.J. Geurts, Interacting errors in large-eddy simulation: a review of recent developments, J. Turbul. 7 (5) (2006) 1–16.
[43] R.S. Rogallo, P. Moin, Numerical simulation of turbulent flows, Ann. Rev. Fluid Mech. 16 (1984) 99–137.
[44] C.D. Pruett, Toward the de-mystification of LES, in: Proceedings of the 3rd AFOSR International Conference on DNS/LES, Arlington (TX), USA, 2001.
[45] G. Comte-Bellot, S. Corrsin, The use of a contraction to improve isotropy of grid generated turbulence, J. Fluid Mech. 25 (1966) 657–682.
[46] J.C. Kok, S.P. Spekreijse, Efficient and accurate implementation of the k-ω turbulence model in the NLR multi-block Navier–Stokes system, in: ECCOMAS 2000, Barcelona, Spain, 2000, NLR-TP-2000-144.
[47] P. Wesseling, Principles of computational fluid dynamics, No. 29 in Springer Series in Computational Mathematics, Springer-Verlag, Berlin, 2001.